CASING CAPACITY DEGRADATION OF BURST AND COLLAPSE OF A NON- UNIFORM CASING WITH WEAR UNDER BENDING CONDITIONS

A Thesis

Presented to

The Faculty of the Department

Of Petroleum Engineering

University of Houston

In partial fulfillment

Of the requirements for the degree

Master of Science

In Petroleum Engineering

By

Dileep Kumar Ujjineni

December 2016

CASING CAPACITY DEGRADATION OF BURST AND COLLAPSE OF A NON- UNIFORM CASING WITH WEAR UNDER BENDING CONDITIONS

Dileep Kumar Ujjineni

Approved:

Chair of the Committee
Dr. Mohamed Y. Soliman, Department Chair
Petroleum Engineering, University of Houston

Committee Members:

Dr. Robello Samuel, Adjunct Faculty
Petroleum Engineering Department
University of Houston

Dr. Cumaraswamy Vipulanandan, Professor
Civil and Environmental Engineering,
University of Houston

Dr. Suresh K. Khator, Associate Dean
Cullen College of Engineering
University of Houston

Dr. Mohamed Soliman, Department Chair
Petroleum Engineering Department
University of Houston

ACKNOWLEDGMENTS

I thank my supervisor, Dr. Robello Samuel, for taking me on as his student and for his advice and understanding throughout the duration of my degree.

I thank Dr. Mohamed Soliman for agreeing to chair the committee and Dr. Cumaraswamy Vipulanandan for agreeing to be a member of my thesis defense committee.

Thanks to my family for their support, understanding, and love. Finally, I am immensely grateful to my fiancé, Akhila for her incredible help and motivation with which I could not have completed this project.

CASING CAPACITY DEGRADATION OF BURST AND COLLAPSE OF A NON- UNIFORM CASING WITH WEAR UNDER BENDING CONDITIONS

An Abstract

Presented to

The Faculty of the Department

Of Petroleum Engineering

University of Houston

In partial fulfillment

Of the requirements for the degree

Master of Science

in Petroleum Engineering

By

DILEEP KUMAR UJJINENI

December 2016

ABSTRACT

Casing wear during drilling and workovers is a major concern in deep or extended reach wells. Wear by drill string results in thinner portion of casing wall which causes reduction of casing strength. Wall thinning could also be caused by bending of casing at steep trajectories. It is important not only to estimate the casing wear but also to reassess the strength of the residual casing due to combined effect non uniform thickness due to bending and wear. The API equations describing casing burst and collapse capacities do not address casing response with geometrical defects such as wear, wall thinning and combined loads. A common methodology is to estimate the reduction of strength from API burst and collapse equations with a linear reduction by remaining wall thickness or wear percentage equivalent to a “uniformly – worn” casing model to reassess casing strength for worn casing. However, this strength estimation is a very conservative method. Therefore, it is required to predict the safe working pressures for casing for the mentioned scenarios. This study presents new analytical models to calculate the degraded burst, collapse and bending strengths for a non- uniform casing with “crescent-shape” casing wear.

These models can be used together to calculate the overall stress profile of a casing with wear, corrosion or cracks to get an estimate of the degradation of the strength. A parametric study of the casing wear percentage, wear radius, and non-uniformity has been performed. The analytical models have been validated by a numerical simulator FEM which uses finite element technique.

TABLE OF CONTENTS

LIST OF FIGURES

LIST OF TABLES

NOMENCLATURE

OD = Outer diameter of casing, in

R_0 = Outer radius of casing, in

t = Nominal thickness of casing, in

t_a = Minimum thickness of casing at point A, in

t_b = Maximum thickness of casing at point B, in

t_a' = Minimum thickness of casing at point A after wear, in

t_c = Thickness of casing at any point C, in

r_s = Wear circle radius, in

α_0 = Half angle made by casing wear at the center of wear circle, degrees

θ_0 = Half angle made by casing wear at the center of casing, degrees

d = Distance between centers of wear circle and outer casing, in

x_i = Inner radius profile function of casing, in

y_i = Inner radius profile function of casing wear w.r.t center of outer casing, in

β = Half angle made by neutral axis at the center of outer radius circle, degrees

β' = Half angle made by neutral axis at the center of inner circle, degrees

M = Bending moment on the cross section of a casing, in-kips

I = Areal moment of inertia, in^4

y = Distance measured from neutral axis, in

h = Modified thickness of casing, in

σ_a = Average hoop stress of casing at minimum thickness, psi

σ_b = Average hoop stress of casing at maximum thickness, psi

σ_{xx} = Axial stress in X direction of a casing, psi

ϵ = Deflection of casing at any point on casing, in

ϵ_0 = Maximum deflection of casing, in

R_m = Radius of the mean circle, in

M_c = Moment at point C, in-kips

E = Young's Modulus, psi

ν = Poisson's ratio, dimensionless

1 INTRODUCTION

1.1 Problem Statement

Casing wear during drilling and workovers is a major concern in deep or extended reach wells. The integrity of casing is very important specifically in wells with casing wear. Casing wear by drill string results in thinner portion of casing wall and a reduction on casing burst, collapse strengths. Wall thinning could also be caused because of bending of casing at steep trajectories. The important issue in oil and gas industry is to estimate the reduced casing burst and collapse strength due to combined effect of wear and bending. The API equations describing casing burst and collapse limits do not address casing response with geometrical defects such as wear, wall thinning and combined loads. A common methodology is to estimate the reduction of strength from API burst and collapse equations with a linear reduction by remaining wall thickness or wear percentage equivalent to a "uniformly – worn" casing model to reassess casing burst strength for worn casing. However, this strength estimation is a very conservative method. So, it is required to predict the safe working pressures for casing for the expected scenarios.

1.2 Background and Literature Review

The literature in Table 1 has been reviewed before developing the analytical models. Various models for Burst, Collapse and bending have been developed in general for a long symmetric cylindrical shells long back. There are few other models proposed considering the degradation of strength due to casing wear of a uniform casing. However, till date no reliable model has been developed to estimate the casing strength degradation for burst, collapse and bending strengths of a non-uniform casing with "crescent-shape" wear. Table 1 contains the list of published literature of the topic under study.

Table 1 - Summary of literature review.

Research Paper	Author	Discipline
Casing Wear Factors: How do They Improve Well Integrity Analyses?	Kumar, A., & Samuel, R. (2015, March 17)	Drilling
Casing Integrity: Modeling Strength Degradation.	Li, C., & Samuel, R. (2016, March 1)	Drilling
Casing Burst Strength After Casing Wear.	Wu, J., & Zhang, M. (2005, January 1)	Drilling
A Theoretical and Experimental Approach to the Problem of Collapse of Deep-Well Casing	Holmquist, J. L., & Nadai, A. (1939, January 1)	Drilling
Effect of Stress Concentration Factors due to Corrosion on Production Tubing Design	Sun, K., Samuel, R., & Guo, B. (2004, January 1)	Drilling
Effect of Wear and Bending on Casing Collapse Strength.	Kuriyama, Y., Tsukano, Y., Mimaki, T., & Yonezawa, T. (1992, January 1)	Drilling

Table 1 (continued)

Combining Bending and Hoop Stresses to Determine Collapsing Pressure of Oil-Country Tubular Goods	Main, W. C. (1939, January 1)	Drilling
Structural modeling of the casings in high temperature geothermal wells	Kaldal, G.S., Jonsson, M.T., Palsson, H. and Karlsdottir, S.N., (2015)	Drilling
Theory of elastic stability	Timoshenko SP, Gere JM (1991)	Drilling
A New Empirical Formula for Collapse Resistance of Commercial Casing	Tamano, T., Mimaki, T., and Yanagimoto, S (1983)	Drilling
A Rational Expression for the Critical Collapsing Pressure of Pipe under External Pressure	Clinedinst, W. O. (1939)	Drilling
Plasticity	A. Nadai (1931)	Drilling
Tube collapse under combined external pressure, tension and bending	Bai Y, Igland R, Moan T (1997)	Drilling
A New Formula for Elasto-Plastic Collapse Strength of Thick-Walled Casing	Kuriyama, Y. (1994, January 1).	Drilling

1.3 Objectives

The objectives of this research work are as follows:

1. Develop an analytical solution for calculation of casing burst capacity under combined internal and external pressure with non -uniform thickness and “crescent-shape” wear symmetrical to the bending plane.
2. Develop an analytical solution for calculation of casing bending moment capacity under combined internal pressure, with non -uniform thickness and “crescent-shape” wear.
3. Develop an analytical solution for calculation of collapse capacity under combined internal pressure, with non -uniform thickness and “crescent-shape” wear.
4. Re- asses limit burst, bending and collapse capacities for all the standard industry casing sizes using new proposed models.
5. Perform sensitivity analysis of casing wear percentage in an attempt to understand the rate of strength degradation as a percentage of wear for burst, collapse and bending.
6. Comparison of new proposed analytical solutions with other existing models.
7. Validate the results from the analytical models using FEM software for burst and collapse loading conditions for all the standard casing sizes.

1.4 Thesis Outline

In this study, new analytical models have been proposed to calculate degradation of burst, collapse and bending strengths for a casing with varying thickness and “crescent-shape” casing wear.

Chapter 2 of this study includes the discussion about the factors affecting strength degradation of the casing, effect of wear and effect of bending. It also summarizes the historical formulations developed for basic burst, collapse and bending equations and the current models used in the industry. The limitations of the models and scope of improvement also has been discussed in this chapter.

In chapter 3, an attempt at developing analytical models has been made to achieve best estimate solution to mimic the reality for strength degradation of casing. Models have been developed considering a long casing. A cross section of casing at a deviated section of a well has been evaluated in detail. Parameters have been defined to account for eccentricity due to bending and wear is considered in the shape of “crescent-shape”. Solutions are developed to calculate the degraded casing strength under burst, collapse and bending conditions.

Chapter 4 highlights the development of the numerical model. The output from this model is used to validate the developed analytical model. A two dimensional surface model similar to the geometrical model is created. FEA model characteristics, boundary conditions and loading conditions have been included. Simulations for burst and collapse have been conducted.

In chapter 5, calculations have been done to identify the internal, external and bending moment capacity on commercially used casing sizes using the proposed analytical models. The analytical models for burst, collapse and bending are validated with numerical model using FEM. Subsequently, comparison of the proposed models with the existing strength assessment models is presented. Parametric analysis has been conducted to understand the effect of wear as percentage of casing wall thickness on casing strength. The results of the same have been presented.

2 CASING STRENGTH DEGRADATION

In recent past, numerous casing failure incidents have been reported during shale well completions. Casing failure compromise the well bore integrity and prevents the access of downhole tools. Casing wear during drilling and workovers is a major concern in deep or extended reach wells. The accurate prediction of casing wear is very important for maintaining well integrity and to reduce the development costs associated with casing. To avoid failures and ensure safe operation casing wear has to be detected, measured and the remaining strength of the casing has to be determined. There are many models being used in the industry to accurately estimate the downhole casing wear. Estimating the wear helps in reassessing the strength of the deployed casing. Casing wear by drill string results in wall thinning and degradation of casing strength. Wall thinning could also be caused by bending of casing at steep trajectories. Critical burst, collapse pressures are very crucial in setting depths for casing subjected to external pressure, planning stages for hydraulic fracking and other conditions which can cause casing integrity failure. If the casing is subjected to wear or corrosion or is under combination of loads such as bending, these additional loads have to be taken into consideration to establish the design limits.

Wear resulted from drill string can be evenly distributed, uniformly reducing the wall thickness of the pipe, or concentrated in one area which produces a crescent-shaped wear pattern. This type of wear can happen in both directional wells and 'straight' holes as well. Crescent-shaped wear casing is neither a uniform thickness cylinder, nor a cracked cylinder. conceptually it can be thought of as somewhere in between. The tool joint of the drill string would create an impression on the casing similar to crescent-wear profile. However, if there is any wobble of the drill string, the wear profile would be slightly different. The assumption here is to consider that the drill string makes a perfect circle shaped wear profile on the casing which is called the 'crescent-shaped' wear.

The important problem in oil and gas industry is to estimate the reduced casing burst and collapse strength due to combined effect of wear and bending. A common methodology is to estimate the reduction of strength from API burst and collapse equations with a linear reduction by remaining wall thickness or wear percentage equivalent to a “uniformly – worn” casing model to reassess casing burst strength for worn casing [3]. This approach for estimating casing strength leads to conservative values resulting in over-design.

The API equations describing casing burst and collapse limits do not address response with geometrical defects such as wear, wall thinning and combined loads. These models can be used together to calculate the overall stress profile with wear, corrosion or cracks to get an estimate of the degradation of the strength.

The objective of this study is to derive analytical solutions for maximum burst, collapse and bending strengths of a casing with non-uniform thickness to evaluate the remaining casing strength. The influence of the defective geometry as a wear percentage of the casing thickness on failure pressure is also analyzed. The non -uniform section is the result of wall thinning of the casing due to bending and wear represented in the form of a crescent. The elastic buckling solution we have arrived is an extension of Timoshenko’s solutions for elastic-plastic collapse of a linear elastic, perfectly plastic cylindrical shell subjected to uniform external pressure.

2.1 Burst

Burst loading is caused when the casing is subjected to higher internal pressure than external. This condition can occur during casing pressure integrity tests, hydraulic fracturing, production operations and well control operations. The industry standard used to calculate the maximum limit for burst pressure is based on Barlow equation. The hoop stress (or tangential stress) at the inner wall of the pipe is calculated by using this equation. The pressure which creates a stress

equivalent to yield stress of the casing is called the limit burst pressure. The pressure obtained using this equation is a conservative value, and an assumption is taken that D/t >> 1.

The von Mises theory has been extensively used for burst pressure prediction of tubulars. Normally, combined stress is compared with yield strength, but for transmitting pipes, it was indicated by various stress values. This was so, because many people considered yield strength too conservative for burst prediction and shifted the failure limit into the plastic region even to the tensile strength value.

However, when applying this theory to wells, the yield strength seems to be a more important property then tensile strength, because when it is passed, the structure deforms permanently and beyond acceptable limits. Therefore, as a failure criterion, the point of the initiation of the plastic behavior was chosen. The failure occurs, when the von Mises equivalent stress reaches the yield strength of the material throughout the remaining tube.

API (1994) [9] adopted the equation (1) to calculate internal yield pressure of a pipe. The factor 0.875 represents the minimum wall thickness factor.

$$P = 0.875 * \left(\frac{2\sigma_Y t}{D}\right), \quad (1)$$

where

P = minimum internal yield pressure in psi.

σ_Y = specified minimum yield strength in psi.

t = nominal wall thickness in inches.

D = nominal outside diameter in inches.

A common method to calculate burst strength with wear is to consider a uniform wear reduction inside the casing, thus using the remaining casing wall thickness to substitute into the API model. However, wall thinning effect due to bending of the casing has not been taken into account for burst calculations.

Another widely used model in calculating casing internal pressure capacity is Nadai's model, which gives the internal pressure capacity based on ultimate tensile strength instead of yield strength given as

$$P = \frac{2}{\sqrt{3}} * \sigma_{uts} * ln(k), \quad (2)$$

where

P = minimum internal yield pressure in psi.

σ_{uts} = specified ultimate tensile strength in psi.

k = geometrical stiffness coefficient, dimensionless.

A new model has been proposed by Li and Samuel [1] to estimate the strength degradation of the uniform thickness casing with "crescent-shape" wear. The limit burst pressure using this model is given as

$$P = \frac{0.875\Delta t_2 \sigma_Y [2(r_1 + r_2) + (\Delta t_1 - \Delta t_2)]}{[r_w(1 - cos\theta_0) + r_i(1 - cos\alpha_0)](2r_1 + \Delta t_1) + 2r_w(r_o - r_w - \Delta t_2)(1 - cos\theta_0)}, \quad (3)$$

where

P = Minimum internal yield pressure in psi.

σ_Y = specified minimum yield strength in psi.

t = nominal wall thickness in inches.

D = nominal outside diameter in inches.

Δt_1 = casing wall thickness at complete part in inches.

Δt_2 = remaining casing wall thickness at wear part in inches.

r_w = wear part radius in inches.

θ_0 = half angle of wear part circular arc in wear circle in degrees.

α_0 = half angle of wear part in casing circle in degrees.

2.2 Collapse

Casings, tubulars are vulnerable to local buckling under external hydrostatic pressure. The loss of integrity can result in huge economic loss. Higher external pressure than internal pressure results in the collapse of the casing. This condition may occur during expansion of trapped fluid, cementing operations, etc. Pipes widely used in oil industry have diameter-to-thickness ratios in the range of 12.5 – 30. Under high external pressure, long pipes tend to fail due to instability at limit pressure. This limit pressure is directly related to the initial ovality and geometrical imperfections of the pipe. Other factors that would influence the collapse behavior are material properties, residual stress and strain hardening parameters. The buckling of thin pipes is determined by the elastic behavior of pipe material, and thicker pipes in the plastic range. The classic collapse equation has been derived by Timoshenko and Gere [8] for elastic buckling of a long cylindrical shell.

The collapse strength equations currently used in the industry provided in API Bull. 5C3 [9] are not developed with considerations such as casing wear, non-uniform thickness, and initial imperfections. Casing design requirements have been increasing especially for deep wells to resist collapse under external pressure while significant internal pressure and axial tension may exist at the same time [10]. The average collapse formulation is given in Bull. 5C3 is a relatively poor predictor of true collapse strength, and therefore need to develop a model which include the effect of wear, non-uniform thickness, corrosion, and other practical conditions, that could adequately capture of the physics of collapse failure.

Under external pressure, round pipe starts to ovalize, and flattens as soon it reaches maximum capacity. A simple equation cannot represent this unstable phenomenon. However, many researchers have presented insights and developed an approximate solution to the collapse equation. The problem of collapse of cylindrical tubes under external pressure is similar to that of

lateral buckling of compressed bars. If the eccentricities are small, the flattening increases slowly and remains negligible to a pressure approaching critical value as calculated by perfectly circular tube. But if the eccentricity is not small, the flattening may be considerable at a comparatively small pressure, and the tube collapses at a pressure much lower than that calculated for a round tube [4]. The effect of ovality of the tube on collapse pressure has been dealt with the fact that the pressure acts on the outside of the tube, and not on the center line of the tube section.

The topic of the collapse of pipes is far from new, and many analytical and numerical approaches have been published. In this study, analytical model has been developed for elastic collapse of a non-uniform worn casing. Elastic collapse is applicable to thin-walled pipe (D/t >>1) and is based on theoretical elastic instability failure criterion. This criterion does not depend on the yield strength of the material. However, it is dependent on initial imperfection such as ovality, eccentricity, Diameter to thickness ratio, and material properties such as stress-strain curve and residual stresses of the material. The collapse strength of the casing can be increased by following better manufacturing standards. Some of the existing models for elastic collapse of an ideal pipe which are related to this discussion are given below:

The collapse problem of a uniform thin cylindrical shell has been solved by Timoshenko, 1931 using the elastic theory. His approach is widely used by other researchers to provide the solution for thick walled cylinder. Industry uses the collapse pressure formula derived from the theoretical elastic pressure formula developed by W.O. Clinedinst, 1939 given in equation (4)

$$P = \frac{2E}{1-\nu^2} \mathrm{x} \frac{1}{\left(\frac{D}{t}\right) \mathrm{x} \left[\left(\frac{D}{t}\right) - 1\right]^2}, \tag{4}$$

where

E = Elastic modulus in psi.

ν = poisson's ratio, dimensionless.

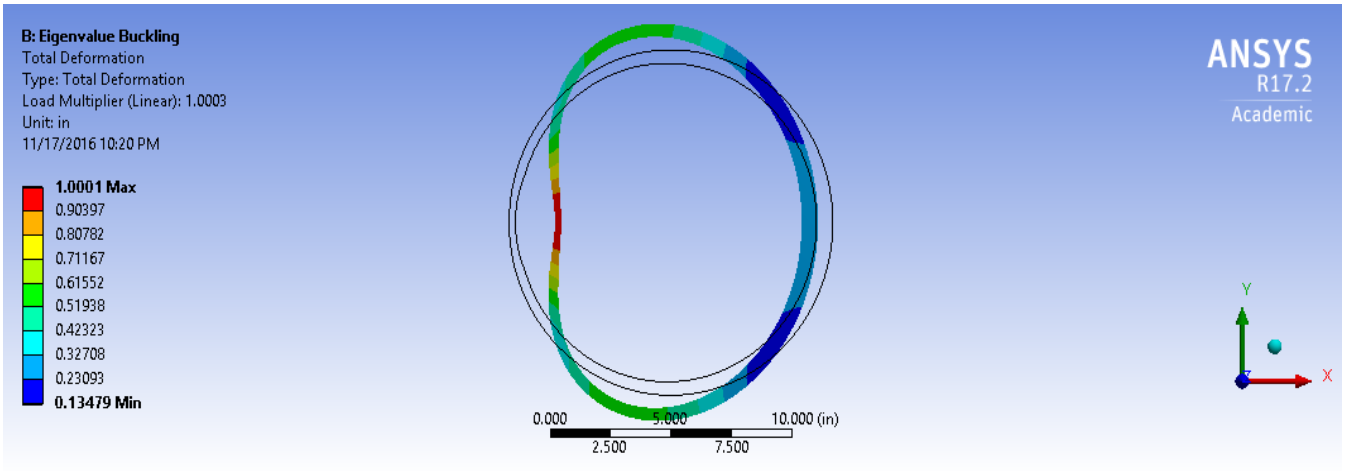

Figure 1: Collapse failure of casing

Collapse prediction is more difficult, because failure occurs under elastic, elastic-plastic or plastic deformation [10]. It is also very sensitive to geometric imperfections such as pipe ovality or corrosion defects. Failure prediction occurs in a similar way to the burst failure prediction presented above. Material behavior is modelled in elastic and plastic regions with work hardening. Stresses are also compared to the von Mises yield criterion. The main difference is that the created procedure stops if instability occurs or the equivalent von Mises stress exceeds, at any point of the pipe, the yield strength through the wall. For visualization purposes further stages of the collapse analysis is shown below in Figure 1. The empirical equations developed for collapse resistance are based on theoretical, numerical and statistical methods. These equations do not account for external casing support and non-uniform loads along the casing and so considered to be rather conservative.

The ratio of outer diameter to thickness (D/t) is considered as a parameter to determine whether collapse occurs in the elastic-, plastic- or intermediate range of the wall compressive stresses. For high values of the D/t ratio, elastic collapse is a governing factor. For lower values, the buckling occurs in the plastic range and for the lowest values the buckling is governed by the yield strength of the material (10400:2007(E) 2007). The critical elastic buckling pressure for long tubes under uniform radial pressure is (Timoshenko, 1961) where v is Poisson's ratio, E is Young's

modulus, t is the tube thickness and R is the tube radius. This equation does however not account for collapse as a result of plastic deformation in the material which occurs in thicker casings. For thicker casings a tangent modulus, Et is used in place of E, to find the critical buckling pressure beyond the proportional limit.

As per API Bull 5C3 [9], theoretical studies of the effect of ovality on collapse resistance consistently indicate that an ovality of 1 to 2 percent can effect a reduction in collapse reduction on the order of 25 percent. However, a much smaller effect is indicated in experimental/empirical investigations. Experimental test data concludes that ovality is one of many pipe parameters that influence collapse. However, it is not the single most dominant parameter. An API work group on collapse resistance concluded the effect of ovality o tubular collapse has been handled during the adjustment of average collapse predictions. But, experimental test data and numerical simulations are not in agreement with API average collapse equation.

2.3 Bending

In highly deviated wells, casing is subjected to bending. Bending on the casing can decrease the casing performance. The reduction of limit burst and limit collapse due to bending has to be taken into consideration during the design process. Effects of Bending such as eccentricity, ovality and axial stresses have to be taken into account. Bending increases ovality and eccentricity which reduces the casing strength. Limit burst pressure is reduced due to thinning of casing wall and limit collapse pressure due to ovality. Axial stress also would reduce the collapse strength.

2.4 Casing wear

The strength of a worn casing depends on two important factors. These are the wear distribution and eccentricity of the tube middle surface. Casing worn can happen in two ways, large amount of wear at a region or small wear over the entire casing. With equal minimum and original wall thickness, casing with wider distribution of wear would have a lower collapse

pressure. If the wear occurs equally on inner and outer casing, the effect of eccentricity on collapse would be negligible. A casing with uniform wall thickness would also have eccentricity. Casing wear occurs inevitably in the drilling process. It not only reduces the wall thickness of the pipe but also decreases the casing strength. These can cause drilling failure accidents, environment damage, and even premature abandonment of the well. As a result, the petroleum industry is estimated to spend tens of millions of dollars each year on extra casing thickness to allow for wear. It is shown from the literature and field predictions that the crescent-shape wear pattern is the most common wear type.

2.5 Linear and Non Linear Buckling

The linear buckling analysis in FEA also called as Eigen buckling is directly related to the classic Euler type of calculation. A small displacement of a disturbed or imperfect shape is assumed in each element that induces a stress dependent stiffening effect. This adds to the linear static stiffness in the element. The stress dependent stiffness is now subtracting from the linear static stiffness term. This latter effect causes linear buckling. In an assembly of elements in an FEA model there will be a subtle interaction between the original linear stiffness matrix and the stress dependent stiffness matrix. This is analogous to the linear stiffness matrix and the mass matrix in a normal modes analysis. The same solution method is used — an eigenvalue extraction. Eigenvalue analysis predicts the theoretical buckling strength of a structure which is idealized as elastic. For a basic structural configuration, structural eigenvalues are computed from constraints and loading conditions. For a linear buckling analysis, this will find what scaling factors applied to the nominal static load will scale the stress stiffening terms to subtract sufficiently from the linear static terms to give unstable solutions. This scaling factor in FEM is called load multiplier.

If for any reason the results of a linear buckling solution suggest the calculation is not representing the real response, then a nonlinear buckling analysis is called for. This uses a

nonlinear geometric analysis to progressively evaluate the transition from stable to unstable and addresses many of the limitations we have seen in linear buckling analysis. Nonlinear buckling analysis provides greater accuracy than elastic formulation. Applied loading incrementally increases until a small change in load level causes a large change in displacement. This condition indicates that a structure has become unstable. Nonlinear buckling analysis is a static method which accounts for material and geometric nonlinearities and geometric imperfections. Either a small destabilizing load or an initial imperfection is necessary to initiate the solution of a desired buckling mode.

3 ANALYTICAL MODEL DEVELOPMENT

3.1 Burst Capacity – Non -uniform casing wall thickness

Consider a long cylindrical casing of outer radius R_o as shown in Figure 2. A cross section of the casing in the deviated hole at section X-X is represented as shown in Figure 2. Bending of the casing results in varying thickness in this cross-section. As observed, the minimum thickness t_a is at point A and maximum thickness t_b is expected to be at its diametrically opposite point B.

3.1.1 Assumptions and Limitations

The assumption in developing this model is that the wear occurs at the thinnest section of the

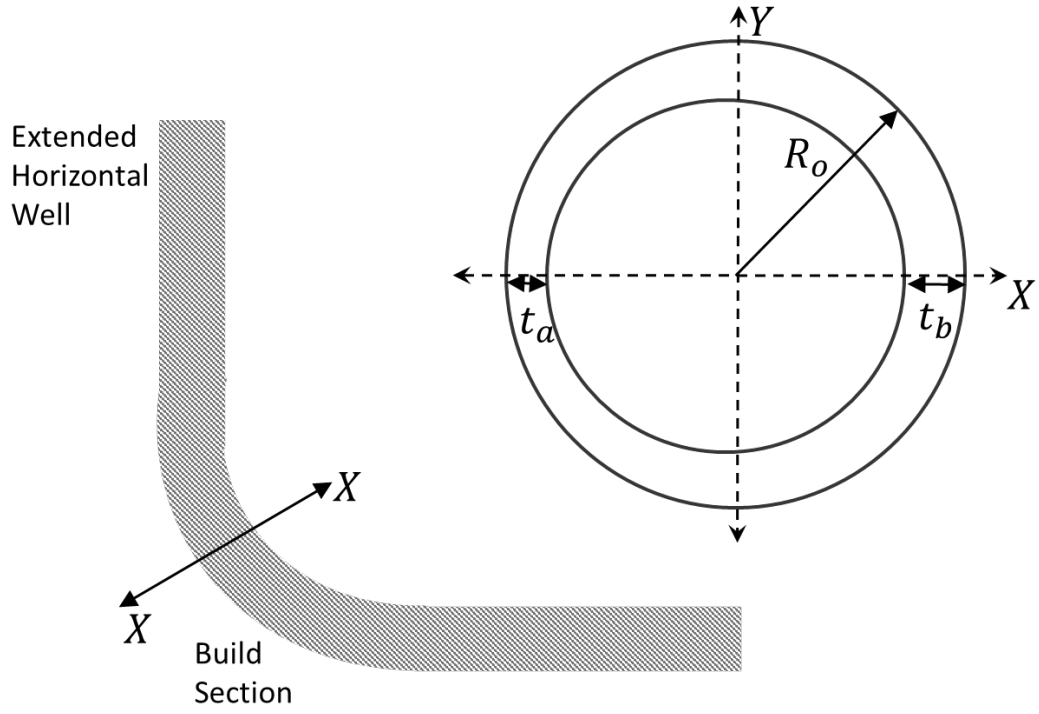

Figure 2: Bent cross-section of an extended horizontal well showing non-uniform wall thickness

non - uniform casing caused due to bending. The outer radius of casing is constant and thickness variation is caused by the varying the inner profile. Wear is introduced by superimposing wear circle on non-uniform circle. The burst, collapse and bending capacities have been evaluated individually without using combined loading.

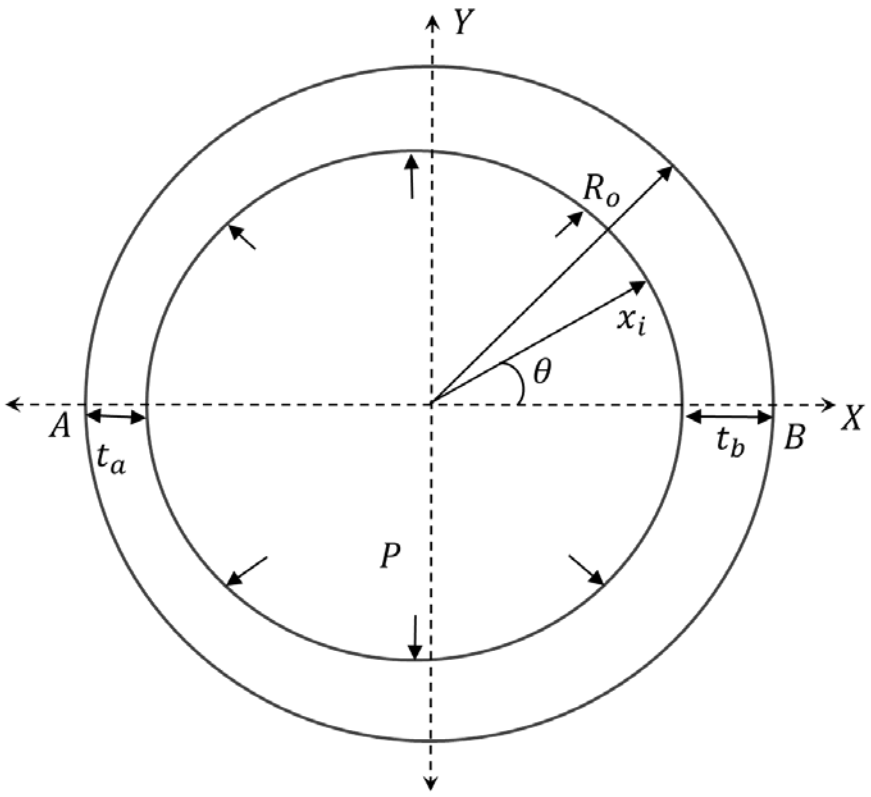

Figure 3: Cross-section of a casing with non-uniform wall thickness with internal pressure

For a casing with non -uniform thickness as shown in Figure 3 and subjected to internal pressure, the hoop stress on thinner wall will increase comparing to casing with uniform wall thickness. Since the casing wall thickness at a cross-section is not constant, the inner radius x_i of the casing is a function of θ and can be traced by using equation (5). Here, θ is the angle considered in anti-clock wise direction i.e. from point B to point A. The inner radius is given in equation (5) as

$$\mathrm{x_i} = \mathrm{f}(\theta) = \mathrm{a}\theta + \mathrm{b}. \tag{5}$$

Constants a and b can be obtained by using the boundary conditions in equation (6)

$$\mathrm{x_i} = \begin{cases} \mathrm{R_o} - \mathrm{t_b} & \text{at } \theta = 0 \\ \mathrm{R_o} - \mathrm{t_a} & \text{at } \theta = \pi. \end{cases} \tag{6}$$

The inner wall of the casing can be traced by equation (7)

$$x_i = (t_b - t_a)x\frac{\theta}{\pi} + (R_o - t_b). \quad (7)$$

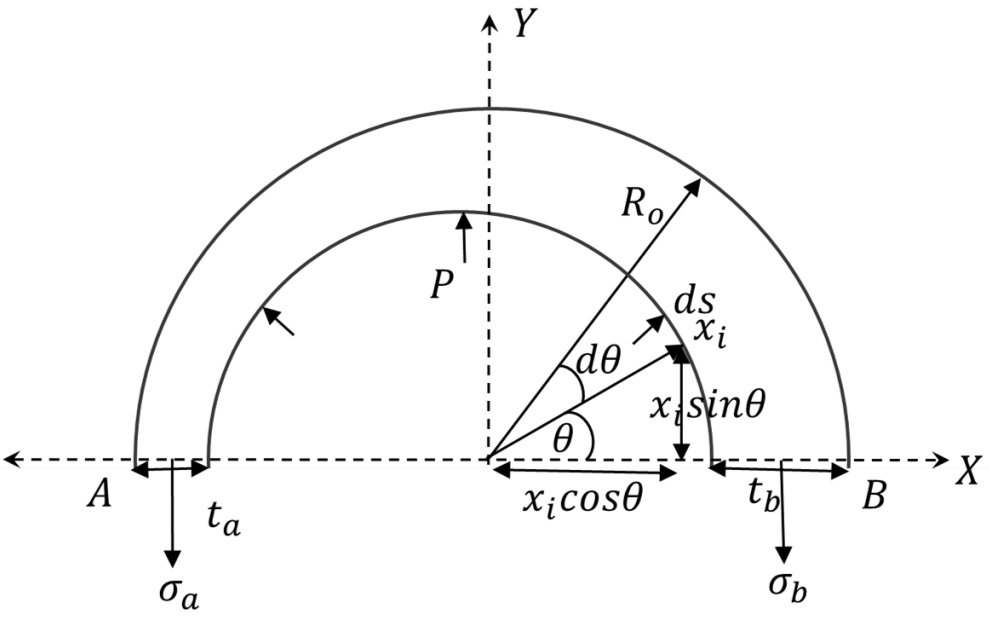

Figure 4: Free body diagram of casing under burst

The differential between internal and external pressures, P is applied on the inner surface of the casing. Due to symmetry along the horizontal axis, only the top half section of the casing is considered. The hoop stresses at point A and point B are σ_a and σ_b respectively as shown in Figure 4. Since commercial casings have D/t>10, thin cylinder assumption can be used. Force balance equation in Y direction can be written as

$$\sigma_a t_a + \sigma_b t_b = \int_0^{\pi} P x_i \, sin\,\theta \, d\theta. \quad (8)$$

By substituting equation (7) in equation (8) and integrating from 0 to π, simplified force equation is expressed as

$$\sigma_a t_a + \sigma_b t_b = P(2R_o - t_a - t_b). \quad (9)$$

At an angle θ, a small differential arc ds subtends an angle $d\theta$ at the center of the casing. The Moment balance equation w.r.t Z axis at center can be written as

$$\sigma_b t_b \left(R_o - \frac{t_b}{2}\right) = \sigma_a t_a \left(R_o - \frac{t_a}{2}\right) + \int_0^{\pi} P x_i^2 \, sin\,\theta \, cos\,\theta \, d\theta. \quad (10)$$

By simplifying equation (10) using x_i and integrating it over the considered half section, the obtained equation is

$$\sigma_a t_a \left(R_o - \frac{t_a}{2}\right) - \sigma_b t_b \left(R_o - \frac{t_b}{2}\right) = \frac{P(t_b - t_a)^2}{4} + \frac{P(t_b - t_a)(R_o - t_b)}{2}. \quad (11)$$

By solving force balance equation (9) and moment balance equation (11), values for σ_a/P and σ_b/P are obtained as

$$\frac{\sigma_a}{P} = \frac{2R_o - t_a - t_b}{2t_a} \; and \quad (12)$$

$$\frac{\sigma_b}{P} = \frac{2R_o - t_a - t_b}{2t_b}. \quad (13)$$

3.2 Burst Capacity – Non -uniform casing with wear

By following the procedure mentioned in Section 3.1, the hoop stress at points A and B can be derived for casing with wear on the inner wall. The wear is represented by superposition of a circle of radius r_s with the center at a distance d from the casing center. The thickness of casing at point A, t_a' is the least casing thickness resulting in the consideration of worst case condition. α is defined as the angle made by the radius of the wear circle at any point within the wear circle with the horizontal axis and α_o is defined as the angle made by the radius of the wear circle at the point of intersection of casing inner radius and the beginning of wear.

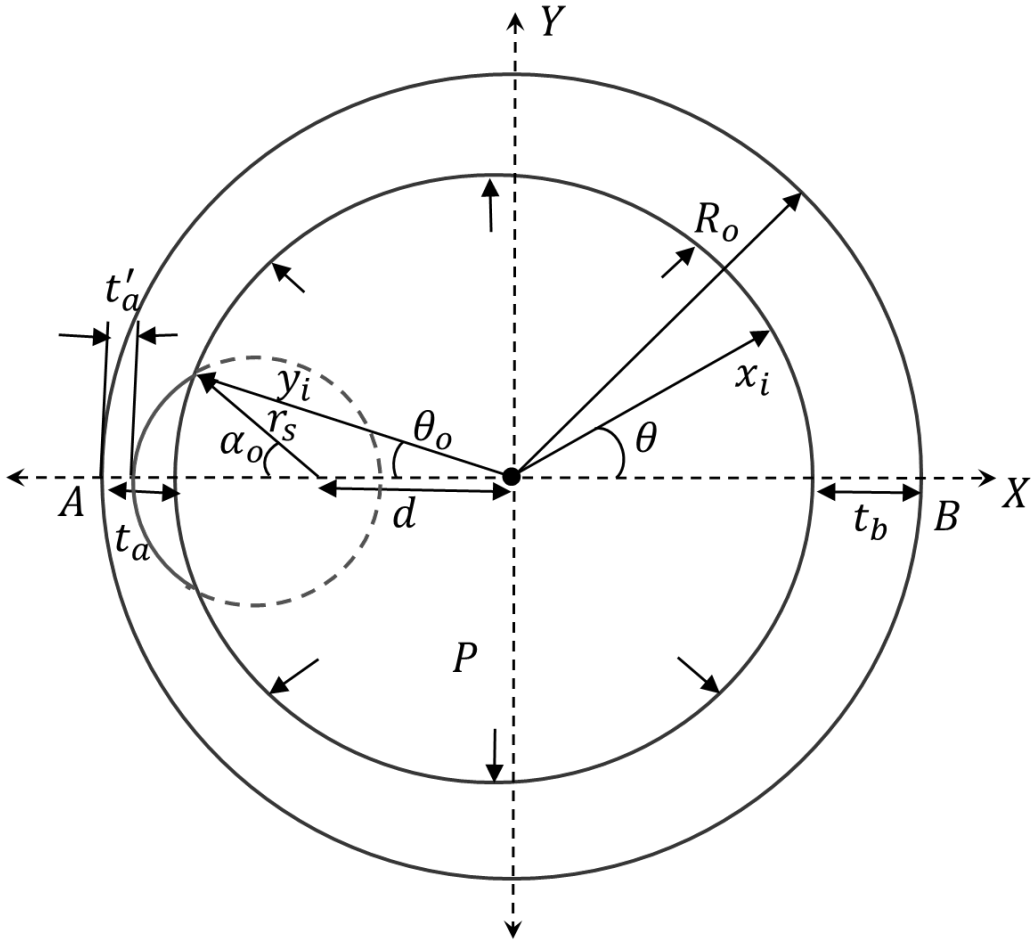

Figure 5: Casing model with non-uniform cross-section and wear under burst

The curve defining the wear region of the casing from the center of the casing is represented by y_i. From Figure 5 y_i can be defined as

$$\mathrm{y_i} \text{ x } sin\,\theta = \mathrm{r_s} \text{ x } sin\,\alpha \;\; and \tag{14}$$

$$\mathrm{y_i} = \frac{\mathrm{r_s} \text{ x } sin\,\alpha}{sin\,\theta}. \tag{15}$$

To calculate θ_o, regression has been done to match x_i and y_i values at the point where casing wear curve meets the inner circle.

The distance between the center of the casing and the center of the wear circle, d is defined as

$$\mathrm{d} = \mathrm{y_i} \text{ x } cos\,\theta_o - \mathrm{r_s} \text{ x } cos\,\alpha_o \;\; and \tag{16}$$

$$\mathrm{d} = \frac{\mathrm{r_s}\ \mathrm{x}\ sin(\alpha_\mathrm{o} - \theta_\mathrm{o})}{sin\,\theta_\mathrm{o}}. \tag{17}$$

Due to additional wear at point A, the thickness of the casing is further reduced to t'_a which is the difference of the outer radius of the casing R_o and the sum of wear circle radius r_s and distance d. t'_a is represented as

$$\mathrm{t'_a} = \mathrm{R_o} - (\mathrm{d} + \mathrm{r_s}). \tag{18}$$

By substituting equation (17) in equation (18), the equation for t'_a in known terms is obtained as

$$\mathrm{t'_a} = \mathrm{R_o} - \mathrm{r_s} - \frac{\mathrm{r_s x}\, sin(\alpha_\mathrm{o} - \theta_\mathrm{o})}{sin\,\theta_\mathrm{o}}. \tag{19}$$

For simplification only the top half circular cross section of the casing has been considered due to symmetry. Force components are integrated over two regions of the casing, one without wear and other with wear. The force component without wear $Px_i \sin\theta\, d\theta$ is integrating from limits 0 to $\pi - \theta_o$ and the force component in the region with wear $Pr_s \sin\theta\, d\theta$ is integrated from limits 0 to α_o. The complete force equation is represented in equation (20) as

$$\sigma_\mathrm{a} \mathrm{t'_a} + \sigma_\mathrm{b} \mathrm{t_b} = \int_0^{\pi-\theta_\mathrm{o}} \mathrm{Px_i}\, sin\,\theta\, \mathrm{d}\theta + \int_0^{\alpha_\mathrm{o}} \mathrm{Pr_s}\, sin\,\theta\, \mathrm{d}\theta. \tag{20}$$

Equations for t'_a and x_i i.e., equations (7) and (19) are substituted in the above force equation (20) and integrated between the limits. Simplified equation is represented as

$$\sigma_\mathrm{a} \mathrm{t'_a} + \sigma_\mathrm{b} \mathrm{t_b} = \mathrm{P}[\mathrm{r_s}\,(1 - cos\,\alpha_\mathrm{o}) + (\mathrm{R_o} - \mathrm{t_b})\,(1 + cos\,\theta_\mathrm{o}) + \mathrm{t_{ab}C}/\pi], \tag{21}$$

where $t_{ab} = t_b - t_a$

Similarly, the moment equation obtained for the top half circular cross-section of the casing is given in equation (22) as

$$\begin{aligned}\sigma_\mathrm{a} \mathrm{t'_a} \left(\mathrm{R_o} - \frac{\mathrm{t'_a}}{2}\right) = \sigma_\mathrm{b} \mathrm{t_b} \left(\mathrm{R_o} - \frac{\mathrm{t_b}}{2}\right) + \int_0^{\pi-\theta_\mathrm{o}} \mathrm{Px_i}^2\, sin\,\theta\, cos\,\theta\, \mathrm{d}\theta \\ + \int_0^{\alpha_\mathrm{o}} \mathrm{Pr_s}\, sin\,\theta\ \mathrm{x}\, \mathrm{y_i}\, cos\,\theta\, \mathrm{d}\theta.\end{aligned} \tag{22}$$

By integrating equation (22) between the limits, the simplified moment equation is given as

$$\sigma_a t'_a\left(R_o-\frac{t'_a}{2}\right)=\sigma_b t_b\left(R_o-\frac{t_b}{2}\right)$$
$$+P\left[\frac{t_{ab}^2\lambda_1}{8\pi^2}+\frac{(R_o-t_b)^2(1-\cos 2\theta_o)}{4}-\frac{t_{ab}(R_o-t_b)\lambda_2}{4\pi}\right. \quad (23)$$
$$\left.+r_s\left(\frac{r_s(\cos^2\alpha_o-1)}{2}-d(\cos\alpha_o-1)\right)\right],$$

where λ_1 and λ_2 are:

$$\lambda_1=[1-2(\pi-\theta_o)^2]\cos 2\theta_o-2(\pi-\theta_o)\sin 2\theta_o-1\ and \quad (24)$$

$$\lambda_2=2(\pi-\theta_o)\cos 2\theta_o+\sin 2\theta_o. \quad (25)$$

By solving the force and moment equations i.e. equations (21) and (23), values for σ_a/P and σ_b/P are obtained.

$$\frac{\sigma_a}{P}=\frac{\psi_1+\psi_2+\psi_3}{t'_a\left(2R_o-\frac{t'_a}{2}-\frac{t_b}{2}\right)}, \quad (26)$$

where

$$\psi_1=P\left[\frac{t_{ab}^2\lambda_1}{8\pi^2}-\frac{t_{ab}(R_o-t_b)\lambda_2}{4\pi}+\frac{t_{ab}\left(R_o-\frac{t_b}{2}\right)\lambda_3}{\pi}\right], \quad (27)$$

$$\lambda_3=(\pi-\theta_o)\cos\theta_o+\sin\theta_o, \quad (28)$$

$$\psi_2=P\left[(R_o-t_b)\left(R_o-\frac{t_b}{2}\right)(1+cos\,\theta_o)+\frac{(R_o-t_b)^2(1-\cos 2\theta_o)}{4}\right. \quad (29)$$
$$\left.+r_s\,(1-cos\,\alpha_o)\left(R_o-\frac{t_b}{2}\right)\right],\ and$$

$$\psi_3=P\left[r_s\left(\frac{r_s(\cos^2\alpha_o-1)}{2}-d(\cos\alpha_o-1)\right)\right]. \quad (30)$$

Upon substituting the value of σ_a/P in equation (21), the value for σ_b/P is given by the equation (31) as

$$\frac{\sigma_b}{P} = \frac{[r_s\,(1 - cos\,\alpha_o) + (R_o - t_b)\,(1 + cos\,\theta_o) + t_{ab}\lambda_3/\pi] - \frac{\sigma_a t'_a}{P}}{t_b}. \quad (31)$$

3.3 Bending Moment Capacity – Non -uniform casing with wear

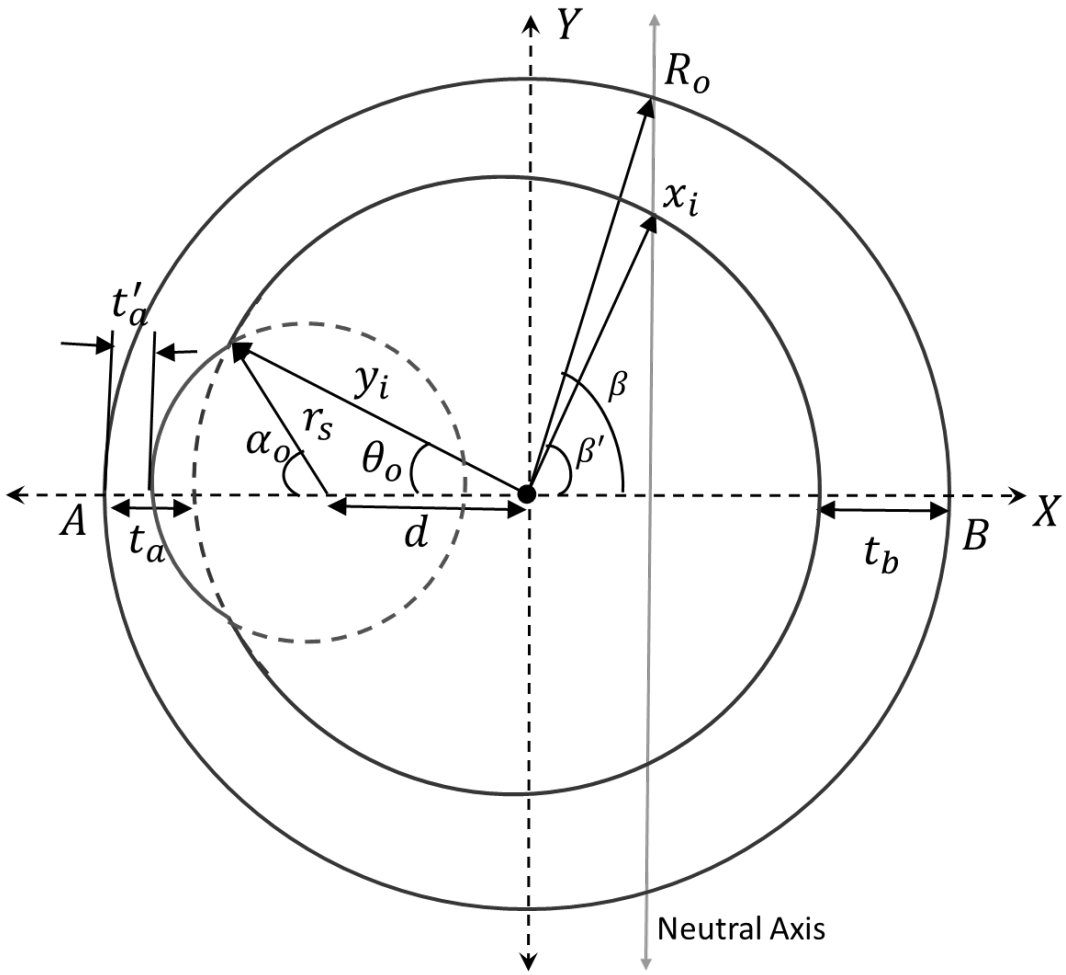

Figure 6: Casing cross-section with non-uniform wall thickness and wear under bending

Bending of the casing causes outer fibers to expand and inner fibers to compress. This results in additional compressive and tensile stresses in inner and outer regions respectively. Due to the non-uniform thickness and casing wear, the neutral axis is not at the center of the casing. The

neutral axis is assumed to be at an angle β from the center of the casing. The inner radius curve makes an angle β' with the neutral axis at the center.

The axial stress (σ_{xx}) at neutral axis would be 0 psi. With the absence of axials loads, the forces on the cross section should be balanced.

As shown in the Figure 6, the right of the neutral axis is under compression. As axial stress increases linearly with distance from the neutral axis y, it is represented as

$$\sigma_{xx} = \begin{cases} 0 & \text{at Neutral axis} \\ \dfrac{My}{I} & \text{at any other location.} \end{cases} \tag{32}$$

The Sum of the forces on the bending plane over an area should be zero and is represented in equations (33) and (34) as

$$\int \sigma_{xx}\, dA = 0, \tag{33}$$

$$\int \frac{My}{I} dA = 0 \text{ , and} \tag{34}$$

$$\int yt\, dy \ \text{(left of NA)} + \int yt\, dy \ \text{(right of NA)} = 0. \tag{35}$$

The Sum of axial force on right of neutral axis should be equal to the force on the left of neutral axis which is formulated in equation (36) as

$$\begin{aligned} &\int_0^{\beta} (R_o\cos\theta - Z)\, R_o\sin\theta\, d(R_o\cos\theta - Z) - \int_0^{\beta'} (x_i\cos\theta - Z)\, x_i\sin\theta\, d(x_i\cos\theta - Z) \\ &= \int_{\beta}^{\pi} (R_o\cos\theta + Z)\, R_o\sin\theta\ d(R_o\cos\theta + Z) \\ &- \int_{\beta'}^{\pi-\theta_o} (x_i\cos\theta + Z)\, x_i\sin\theta\ d(x_i\cos\theta + Z) \\ &- \int_{\pi-\alpha_o}^{\pi} (d + Z + r_s\cos\theta)\, r_s\sin\theta\ d(d + Z + r_s\cos\theta) \end{aligned} \tag{36}$$

(37)

where $Z = R_o cos\beta$

$$\text{Right of Neutral Axis} + \text{Left of Neutral Axis} = 0 \tag{38}$$

But substituting equations (36) and (37) in equation (38), the following equations are obtained as

$$\psi_1 = \frac{-Z\beta'}{3}\left(a^2\beta'^2 + 3ab\beta' + 3b^2\right), \tag{39}$$

$$\psi_2 = \frac{R_o^2 Z}{2}(2\beta - \sin 2\beta - \pi), \tag{40}$$

$$\psi_3 = \frac{Z\sin 2\beta'}{2}(a\beta' + b)^2, \tag{41}$$

$$\psi_4 = \frac{Z\sin 2\theta_o}{4}(a(\pi - \theta_o) + b)^2, \tag{42}$$

$$\psi_5 = \frac{Z(\pi - \theta_o)}{6}[a^2(\pi - \theta_o)^2 + 3ab(\pi - \theta_o) + 3b^2], \tag{43}$$

$$\psi_6 = -a(b^2 - 2a^2) - a\cos\theta_o[a^2((\pi - \theta_o)^2 - 2) + 2ab(\pi - \theta_o) + b^2], \tag{44}$$

$$\psi_7 = \frac{-(a(\pi - \theta_o) + b)\sin\theta_o}{6}[a^2(12 - (\pi - \theta_o)^2) - 2ab(\pi - \theta_o) + (a(\pi - \theta_o) + b)^2\cos 2\theta_o - b^2], \tag{45}$$

$$\psi_8 = \frac{r_s^2}{12}[6\alpha(d + Z) - 3r_s\sin\alpha + r_s\sin 3\alpha - 3(d + Z)\sin 2\alpha]\ , and \tag{46}$$

$$R_o\cos\beta = x_i\cos\beta'. \tag{47}$$

Sum of equations (39) to (46) is equal to zero as shown below in equation (48) as

$$\psi_1 + \psi_2 + \psi_3 + \psi_4 + \psi_5 + \psi_6 + \psi_7 + \psi_8 = 0. \tag{48}$$

The two equations (47) and (48) are solved using regression to obtain the values of β and β'. By obtaining the values of β and β', Moment can be calculated using the below procedure.

Moment equation on either sides of the neutral axis is as shown below:

$$M = \int \sigma_x\, dA * y = k\int y^2\, dy * t\ and \tag{49}$$

$$\int y^2\, t\, dy = \int_0^{\beta} (R_o\cos\theta - Z)^2\, R_o\sin\theta\ \ d(R_o\cos\theta - Z)$$

$$- \int_0^{\beta'} (x_i\cos\theta - Z)^2\, x_i\sin\theta\ \ d(x_i\cos\theta - Z)$$

$$+ \int_{\beta}^{\pi} (R_o\cos\theta + Z)^2\, R_o\sin\theta\ \ d(R_o\cos\theta + Z) \qquad (50)$$

$$- \int_{\beta'}^{\pi-\theta_o} (x_i\cos\theta + Z)^2\, x_i\sin\theta\ \ d(x_i\cos\theta + Z)$$

$$- \int_{\pi-\alpha_o}^{\pi} (d + Z + r_s\cos\theta)^2\ \ r_s\sin\theta\ \ d(d + Z + r_s\cos\theta).$$

By simplifying the above equation (50) and integrating it between the limits, we get the following terms:

$$\psi_1 = \frac{-R_o^4\pi}{4} - \frac{R_o^4\pi}{2} + \frac{4R_o^4}{3}\cos\beta\sin^3\beta, \qquad (51)$$

$$\psi_2 = \frac{1}{160}\{30a^3b$$

$$+ 10a\cos2\theta_o[a^2(2(\theta_o - \pi)^2 - 3) + 4ab(\pi - \theta_o)$$

$$+ 2b^2](a(\pi - \theta_o) + b)$$

$$+ 30a^2\sin\theta_o\cos\theta_o[a^2(2(\theta_o - \pi)^2 - 1) + 4ab(\pi - \theta_o) + 2b^2] \qquad (52)$$

$$+ 4[a^4(\pi - \theta_o)^5 + 5a^3b(\theta_o - \pi)^4 + 10a^2b^2(\pi - \theta_o)^3$$

$$+ 5ab^3(2(\theta_o - \pi)^2 + 1) + 5b^4(\pi - \theta_o)] - 40ab^3$$

$$+ 5\sin4\theta_o(a(\pi - \theta_o) + b)^4\},$$

$$\psi_3 = Z^2\left\{\frac{(\pi - \theta_o)}{6}[a^2(\pi - \theta_o)^2 + 3ab(\pi - \theta_o) + 3b^2]\right. \qquad (53)$$

$$\left. + \frac{\sin2\theta_o}{4}(a(\pi - \theta_o) + b)^2\right\},$$

$$\psi_4 = 2Z\left\{\frac{1}{6}\left[\sin\beta'(a\beta'+b)\left[-a\left(a\left(\beta'^2-12\right)+2b\beta'\right)+\cos2\beta'(a\beta'+b)^2-b^2\right]\right.\right.$$
$$\left.\left.-6a\cos\beta'\left(a\left(\beta'^2-2\right)+2ab\beta'+b^2\right)\right]+a(b^2-2a^2)\right\}, \quad (54)$$

$$\psi_5 = \frac{Z}{6}\left\{-3\sin\beta'(a\beta'+b)\left(a^2-\left(\beta'^2-8\right)+2ab\beta'+b^2\right)\right.$$
$$-12a\cos\beta'\left(a^2\left(\beta'^2-2\right)+2ab\beta'+b^2\right)$$
$$+3\sin\theta_o(a(\pi-\theta_o)+b)[a^2((\pi-\theta_o)^2-8)+2ab(\pi-\theta_o) \quad (55)$$
$$+2b^2]-12a\cos\theta_o[a^2((\pi-\theta_o)^2-2)+2ab(\pi-\theta_o)+b^2]$$
$$\left.+\sin3\beta'(a\beta'+b)^3-\sin3\theta_o(a(\pi-\theta_o)+b)^3\right\},$$

$$\psi_6 = \frac{r_s^2}{96}[12\alpha(4(d+Z)^2+r_s^2)+8(d+Z)(8r_s\sin^3\alpha-3\sin2\alpha(d+Z)) \quad (56)$$
$$-3r_s^2\sin4\alpha],$$

$$M = k\,(\psi_1+\psi_2+\psi_3+\psi_4+\psi_5+\psi_6)\,, and \quad (57)$$

$$I = \psi_1+\psi_2+\psi_3+\psi_4+\psi_5+\psi_6. \quad (58)$$

Maximum tensile stress σ_t and maximum compressive stress σ_c can be obtained from the above equations:

$$\sigma_t = \frac{M}{I}(R_o+\cos\beta)\ and \quad (59)$$

$$\sigma_c = \frac{M}{I}(R_o-\cos\beta). \quad (60)$$

To obtain the bending moment of a uniform cylinder without wear, substitute the geometrical values for casing, with no wear and uniform wall thickness, into the new model. In this case the wall thickness is uniform i.e. $t_a = t_b = t$. since there is no wear in the casing. The neutral axis coincides with the Y-axis which makes the angles β and β' equal to 90 degrees. We obtain values for ψ_1 to ψ_6. We get $\psi_1 = {-R_o^4\pi}/{4}$, $\psi_2 = {R_i^4\pi}/{4}$ and $\psi_3 = \psi_4 = \psi_5 = \psi_6 = 0$. Hence the areal moment of intertia is obtained by the equation $I = {\pi\left(R_o^4 - R_i^4\right)}/{4}$ which is the general equation

for cylindrical cross-section with outer and inner radii as R_o and R_i respectively. By using this areal moment of inertia, the bending moment capacity of a uniform cylinder without wear can be obtained.

3.4 External pressure Capacity – Non -uniform casing with wear

Elastic buckling of a non-uniform cylinder is analyzed in the similar way as the elastic buckling pressure of a uniform cylindrical shell subjected to uniform hydrostatic pressure.

The differential equation for the radial deflection ε of a thin curved bar with circular axis [8] is defined as

$$\frac{d^2\varepsilon}{d\theta^2} + \varepsilon = -\frac{MR^2}{EI}. \tag{61}$$

Flexural rigidity for the circular bar $EI = {Eh^3}/{12}$

A free body diagram for finding the circumferential bending moments of the cylindrical shell is shown in the Figure 8. Moment from the figure can be written as

$$M = M_o + P \times \overline{AO} \times \overline{AB} - \frac{P}{2} \times \overline{AC}^2 \; and \tag{62}$$

$$M = M_o - \frac{P}{2} \times (\overline{CO}^2 - \overline{AO}^2). \tag{63}$$

Assume the deflection at point A as ε_o and deflection at point C as ε. After geometric simplifications, we get the equation for moment as shown in equation (63).

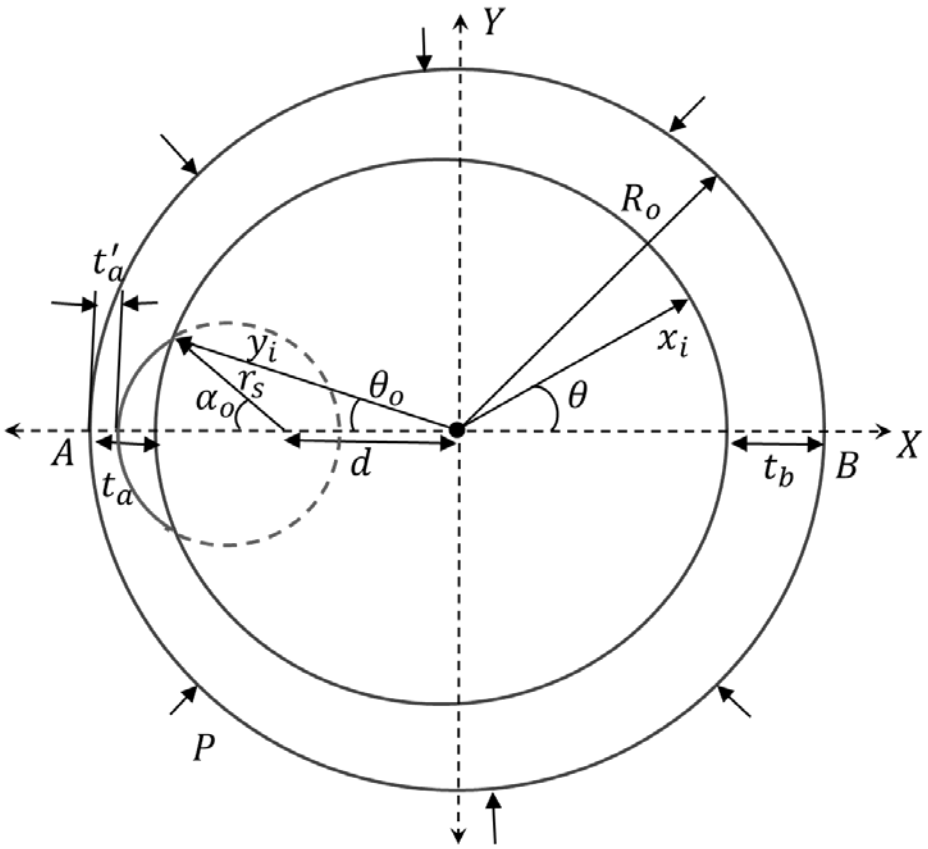

Figure 7: Casing cross-section with non-uniform wall thickness and wear under collapse

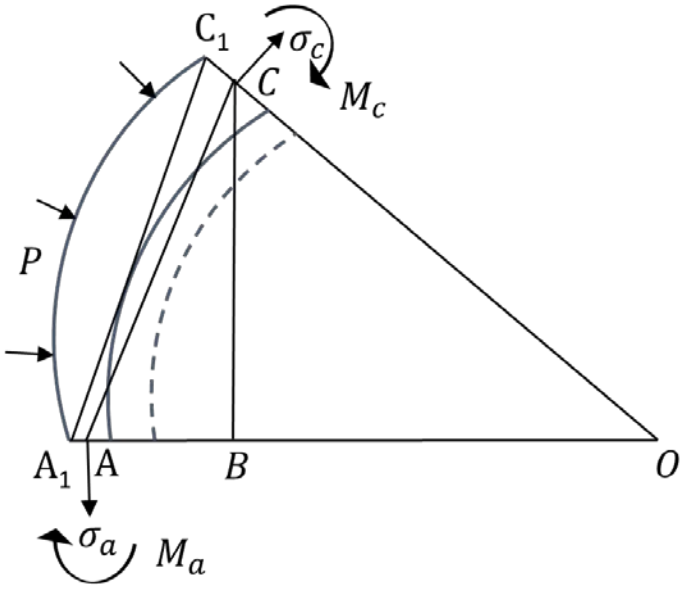

Figure 8: Free body diagram of the section of the casing within the wear circle region

R_m is mean radius of the casing. The geometrical values for $\overline{\mathrm{AO}}$ and $\overline{\mathrm{CO}}$ and M are given by equations (64), (65) and (66) as

$$\overline{\mathrm{AO}} = \mathrm{R_m} - \varepsilon_\mathrm{o}, \tag{64}$$

$$\overline{\mathrm{CO}} = \mathrm{R_m} - \varepsilon \; and \tag{65}$$

$$\mathrm{M} = \mathrm{M_o} - \mathrm{PR_m}(\varepsilon_\mathrm{o} - \varepsilon). \tag{66}$$

Substituting the above equation (66) for the bending moment into the differential equation for radial casing deformation equation (61), it yields the following equilibrium equation for the uniform casing:

$$\frac{\mathrm{d}^2\varepsilon}{\mathrm{d}\theta^2} + \varepsilon = -\frac{12\mathrm{R_m^2}}{\mathrm{Eh^3}}\left(\mathrm{M_o} - \mathrm{PR_m}(\varepsilon_\mathrm{o} - \varepsilon)\right) \; and \tag{67}$$

$$\frac{\mathrm{d}^2\varepsilon}{\mathrm{d}\theta^2} + \left(1 + \frac{12\mathrm{PR_m^3}}{\mathrm{Eh^3}}\right)\varepsilon = -\frac{12\mathrm{R_m^2}}{\mathrm{Eh^3}}(\mathrm{M_o} - \mathrm{PR_m}\varepsilon_\mathrm{o}). \tag{68}$$

Values of R_m and h vary at different regions of the casing as given below:

$$\mathrm{h} = \begin{cases} \dfrac{\mathrm{t_b} + \mathrm{t_c}}{2}, & \text{for } 0 < \theta < \pi - \theta_\mathrm{o} \\ \dfrac{\mathrm{t_a'} + \mathrm{t_c}}{2}, & \text{for } 0 < \theta < \alpha_\mathrm{o} \end{cases} \; and \tag{69}$$

$$\mathrm{R_m} = \begin{cases} \mathrm{R_o} - \left(\dfrac{\mathrm{t_b} + \mathrm{t_c}}{4}\right), & \text{for } 0 < \theta < \pi - \theta_\mathrm{o} \\ \mathrm{R_o} - \left(\dfrac{\mathrm{t_a'} + \mathrm{t_c}}{4}\right), & \text{for } 0 < \theta < \alpha_\mathrm{o} \end{cases}, \tag{70}$$

where, t_c is the thickness of the casing at point C, differentiates the region with wear from the region without wear represented as

$$\mathrm{t_c} = \mathrm{R_o} - \mathrm{y_o} \; and \tag{71}$$

$$\mathrm{y_o} = \frac{\mathrm{r_s}\sin\alpha_\mathrm{o}}{\sin\theta_\mathrm{o}}. \tag{72}$$

The differential equation for radial deformation must now be defined in two regions; one with wear and other without wear region. A general solution of the above second order differential equation (68) for the non-uniform casing is:

$$\varepsilon = \begin{cases} A_1 \sin \lambda_1 \theta + A_2 \cos \lambda_1 \theta + \dfrac{\xi_1}{\lambda_1^2}, & \text{for } 0 < \theta < \pi - \theta_o \\ B_1 \sin \lambda_2 \theta + B_2 \cos \lambda_2 \theta + \dfrac{\xi_2}{\lambda_2^2}, & \text{for } 0 < \theta < \alpha_o, \end{cases} \tag{73}$$

where λ and ξ are:

$$\lambda^2 = 1 + \frac{12PR_m^3}{Eh^3} \; and \tag{74}$$

$$\xi = -\frac{12R_m^2}{Eh^3}(M_o - PR_m\varepsilon_o). \tag{75}$$

A_1, A_2, B_1 and B_2 are constants that depend on the boundary conditions.

The boundary conditions which are needed to evaluate the above integration constants are:

$$\frac{d\varepsilon}{d\theta} = 0, \qquad \text{at } \theta = 0, \pi \tag{76}$$

Slope is continuous at the intersection of two regions given by

$$\frac{d\varepsilon}{d\theta}_{\theta=\theta_o} = \frac{d\varepsilon}{d\theta}_{\theta=\pi-\theta_o}. \tag{77}$$

By substituting the boundary conditions, we get the below values

$$A_1 = 0; \;\; B_1 = B_2 \tan(\lambda_2 \pi). \tag{78}$$

By simplifying the equations using the above obtained values and by substituting the boundary conditions we get the least possible values for λ_1 and λ_2 as

$$\lambda_1 = \lambda_2 = 2.$$

By substituting the values in the equation for λ i.e. equation (74), we get

$$P = \frac{E\left[R_0 - \frac{r_s}{2}\left(1 - cos\alpha_0 - \frac{sin\alpha_0(1 + cos\theta_0)}{sin\theta_0}\right)\right]^3}{4\left[\frac{R_0}{2} + \frac{r_s}{4}\left(1 - cos\alpha_0 - \frac{sin\alpha_0(1 + cos\theta_0)}{sin\theta_0}\right)\right]^3}. \tag{79}$$

4 NUMERICAL SIMULATION MODEL

4.1 Model Geometry

A numerical simulation model is built to simulate loading conditions of the following:

- Average hoop stress estimation to calculate the limit burst pressure of non-uniform casing with wear.
- Elastic collapse buckling pressure estimation of non-uniform casing with wear.
- Nonlinear collapse pressure estimation of non-uniform casing with wear.

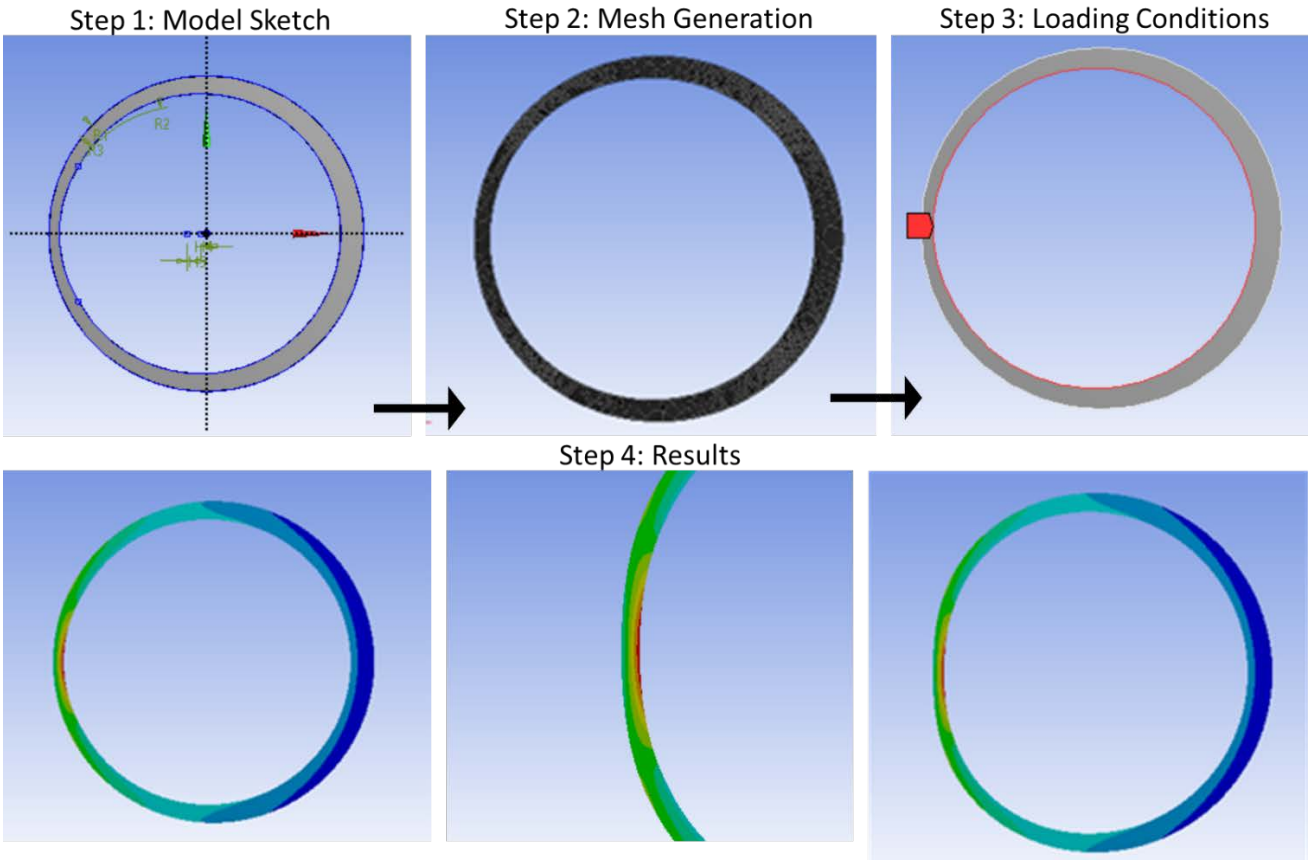

Figure 9: Finite Element Model Development

The finite element method (FEM) is used to construct a two dimensional model of the casing. Eigenvalue buckling analysis is used to predict the theoretical collapse strength and the collapse mode shapes of the casing. The eigenvalue analysis is a linear solution method in which nonlinear

properties, e.g., interaction of contacting surfaces, are not taken into account. Nonlinear buckling analysis is then used to account for nonlinearities properties such as material properties, geometrical displacements. The limit load of the casing is obtained and stabilization is used to track the post buckling shape of the casing. The finite-element program FEM is used to construct the two dimensional model similar to the geometrical model.

4.2 Material Properties and Geometrical dimensions

Industry standard casing sizes from 5" to 13 3/8" have been considered for Finite Element Analysis. The minimum thickness (ta) has been considered as 70% of the nominal thickness to introduce eccentricity. Similarly, the maximum thickness (tb) has been considered as 130% of the nominal thickness. The casing wear circle radius has been selected from the sizes of standard tool joints of drill string.

Table 2: Geometrical information for standard casing sizes

D	Ri	t	rs	ta	tb	D/t
Inches						**-**
5	2.14	0.36	1.80	0.25	0.47	13.81
7	2.96	0.54	2.40	0.38	0.70	12.96
9 5/8	4.27	0.54	2.40	0.38	0.70	17.82
9 5/8	4.27	0.55	3.90	0.38	0.71	17.66
13 3/8	6.17	0.51	4.56	0.36	0.67	26.02

The material properties used in the FE analysis are listed in below:

Property	**Steel**	**Units**
Young's modulus (E)	205	GPa
Poisson's ratio ()	0.3	
Density ()	7850	Kg/m3

4.3 Boundary Condition

4.3.1 Constraints and Symmetry

As the geometry is symmetric along the horizontal axis x-x, a half of the model can be constructed and used to reduce the number of nodes and calculation time approximately 5 fold. The same model can be used for burst and collapse cases. Symmetry can be demonstrated using the Figure 10.

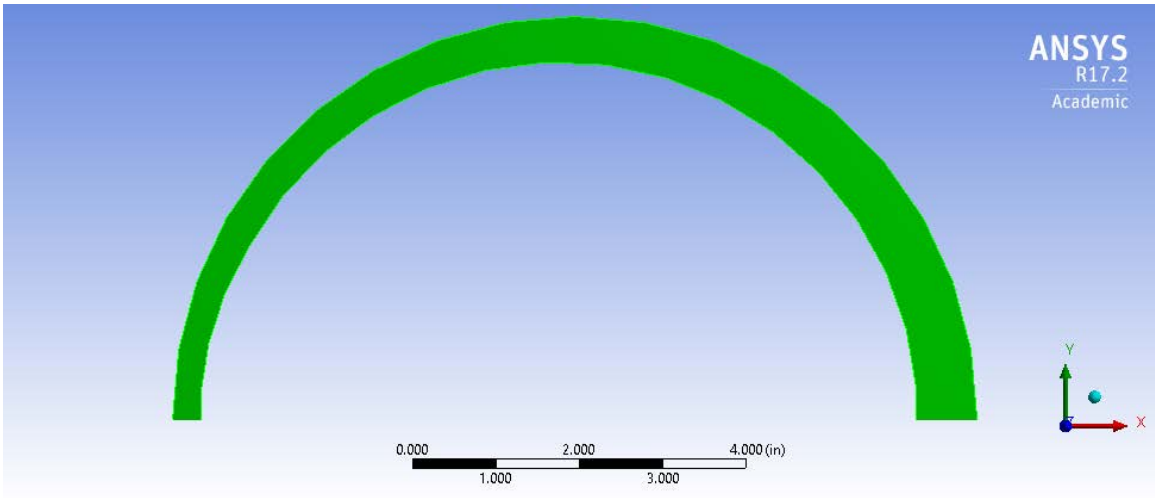

Figure 10: Model with axial symmetry

4.3.2 Applicable Load

Finite Element Model analysis is based on approximations. Model geometry is created to approximate the real shape and constraints approximate how the structure is supported similarly; loads approximate what happens in the real world. Simulations have been performed by applying the following loads on the model:

- Internal pressure on the inner surface (Figure 11)

- External pressure on the outer surface (Figure 12)

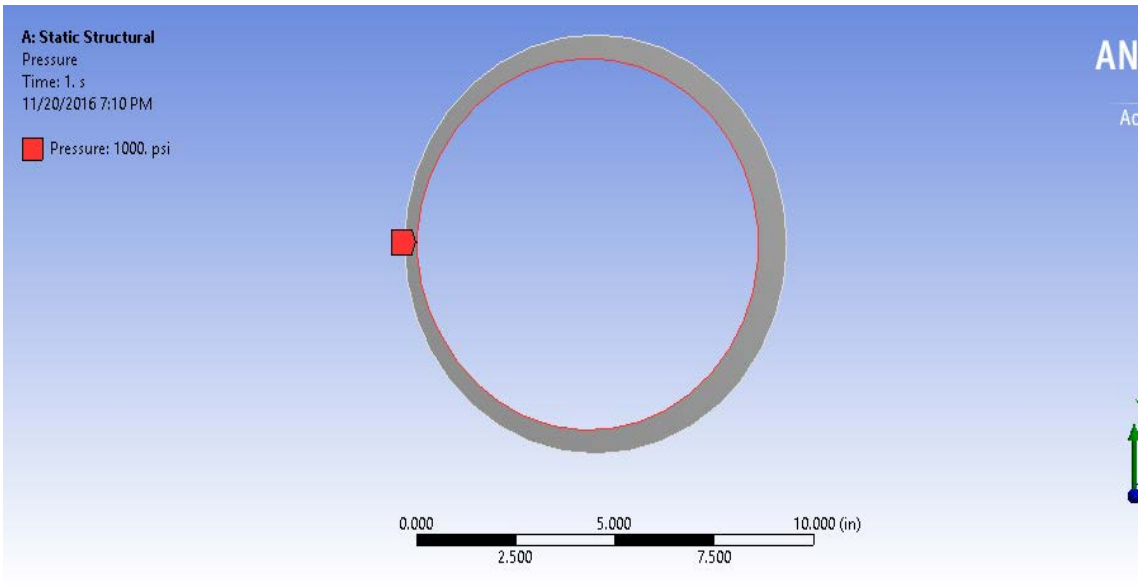

Figure 11: FEA model with internal pressure loading of 1000 psi

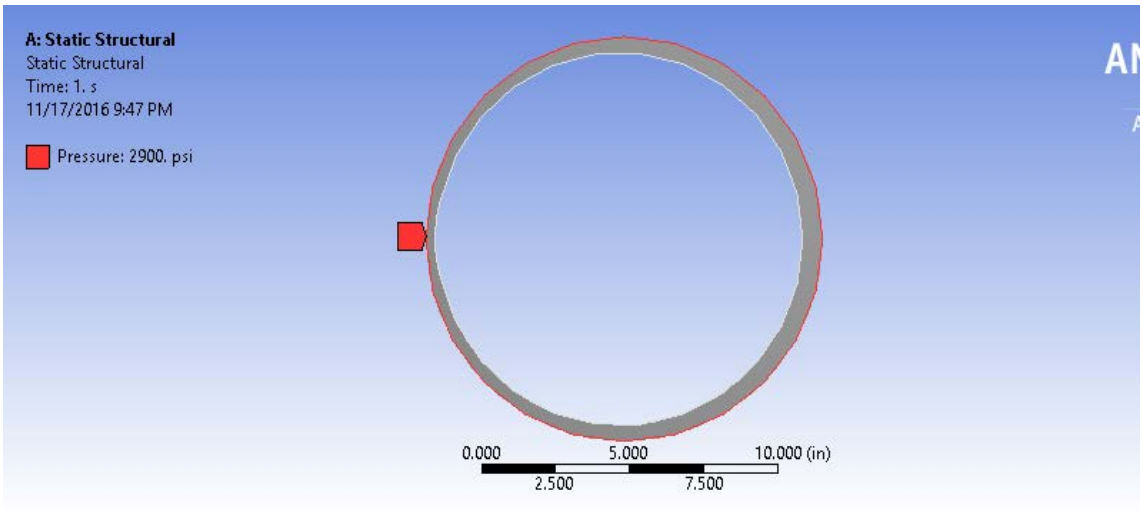

Figure 12: FEA model showing external pressure loading of 2900 psi

The above loads are applied in the numerical model as hydrostatic pressure loads and it is possible to apply them simultaneously. Theoretically, the difference of inner and external pressure is considered the resultant load.

4.3.3 Mesh and Element size

The model has to be subdivided into a finite number of smaller pieces called elements as shown in Figure 13. These elements are defined by points at their edges called nodes. The Finite element mesh is composed of nodes and elements to approximate the shape of the real model. Coarser mesh leads to results which are not accurate but require less computational time. A fine mesh gives results that are closer to the exact solution, but the analysis is more time consuming. However, reducing the element size further does not always guarantee improvement in accuracy of the results. So, an optimized mesh would sufficiently solve the criteria to get good results without consuming more computational time.

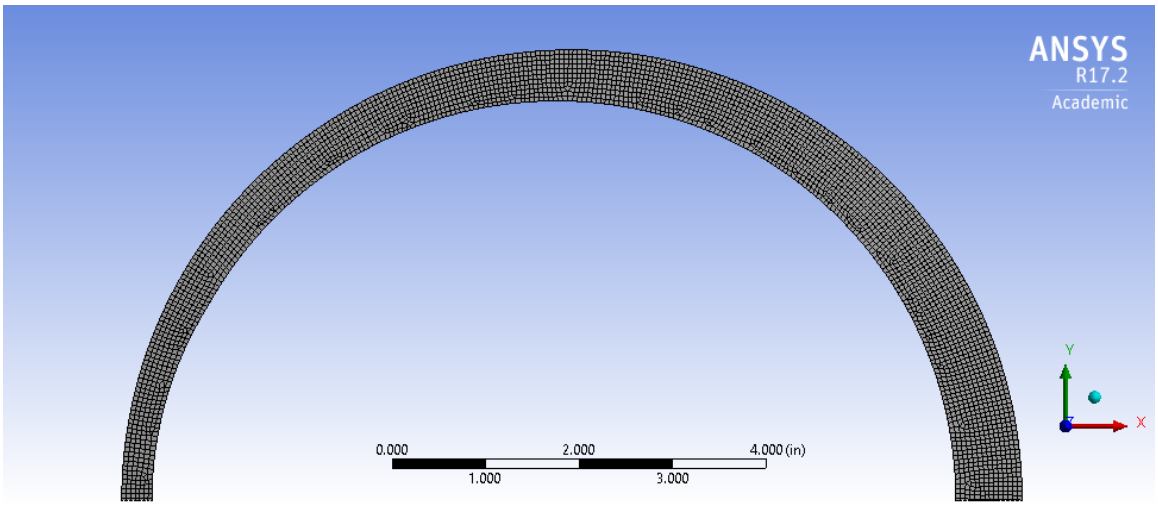

Figure 13: FEA model showing meshing

The element size in each simulation is considered between 0.01 in to 0.06 in depending on the casing size and convergence of solution. Mesh refinement have been implemented to increase local mesh size at regions with significant wear and low thickness. As the stress values in the worn part are relatively important, a judgement call is made to increase the number of elements.

4.4 Eccentricity and Casing wear

As one of the objective of this study is to analyze the effect of eccentricity and wear on casing strength, various models have been created with varying wear and eccentricities. Figure 14 shows a 9 5/8” casing with 20% wear percentages and eccentricity.

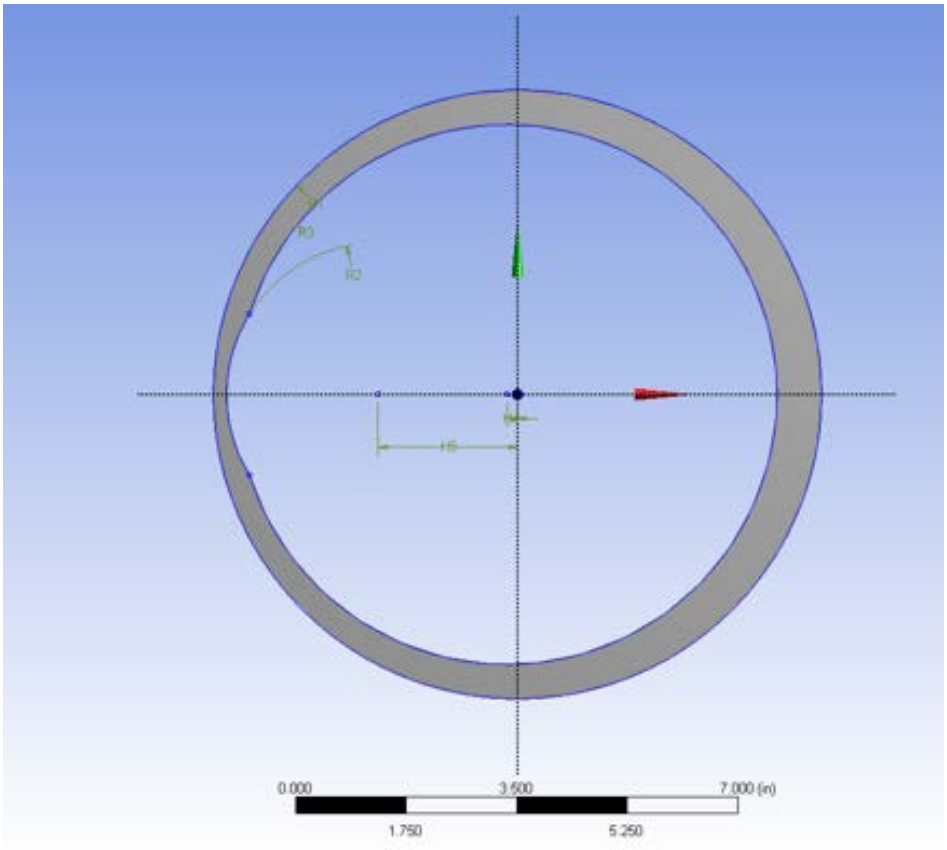

Figure 14: FEM model sketch showing varying casing wall thickness and wear

4.5 Linear and Non Linear Buckling

The linear buckling analysis in FEA also called as Eigen buckling is directly related to the classic Euler type of calculation. A small displacement of a disturbed or imperfect shape is assumed in each element that induces a stress dependent stiffening effect. This adds to the linear static stiffness in the element. The stress dependent stiffness is now subtracting from the linear static stiffness term. This latter effect causes linear buckling. In an assembly of elements in an FEA model there will be a subtle interaction between the original linear stiffness matrix and the stress

dependent stiffness matrix. This is analogous to the linear stiffness matrix and the mass matrix in a normal modes analysis. The same solution method is used — an eigenvalue extraction. Eigenvalue analysis predicts the theoretical buckling strength of a structure which is idealized as elastic. For a basic structural configuration, structural eigenvalues are computed from constraints and loading conditions. For a linear buckling analysis, this will find what scaling factors applied to the nominal static load will scale the stress stiffening terms to subtract sufficiently from the linear static terms to give unstable solutions. This scaling factor in FEM is called load multiplier.

If for any reason the results of a linear buckling solution suggest the calculation is not representing the real response, then a nonlinear buckling analysis is called for. This uses a nonlinear geometric analysis to progressively evaluate the transition from stable to unstable and addresses many of the limitations we have seen in linear buckling analysis. Nonlinear buckling analysis provides greater accuracy than elastic formulation. Applied loading incrementally increases until a small change in load level causes a large change in displacement. This condition indicates that a structure has become unstable. Nonlinear buckling analysis is a static method which accounts for material and geometric nonlinearities and geometric imperfections. Either a small destabilizing load or an initial imperfection is necessary to initiate the solution of a desired buckling mode.

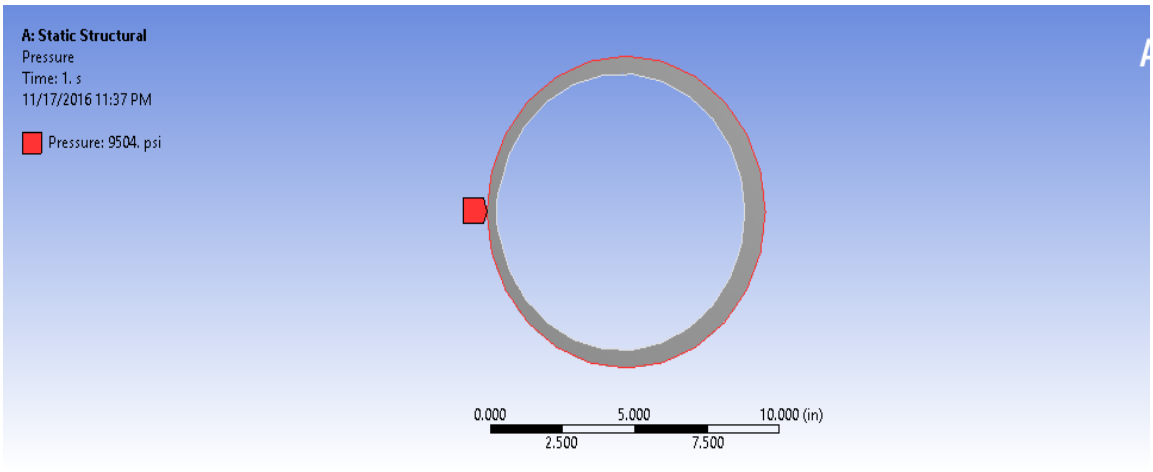

Figure 15: Elastic collapse - Loading condition for 9 5/8" casing with wear as 10% of wall thickness

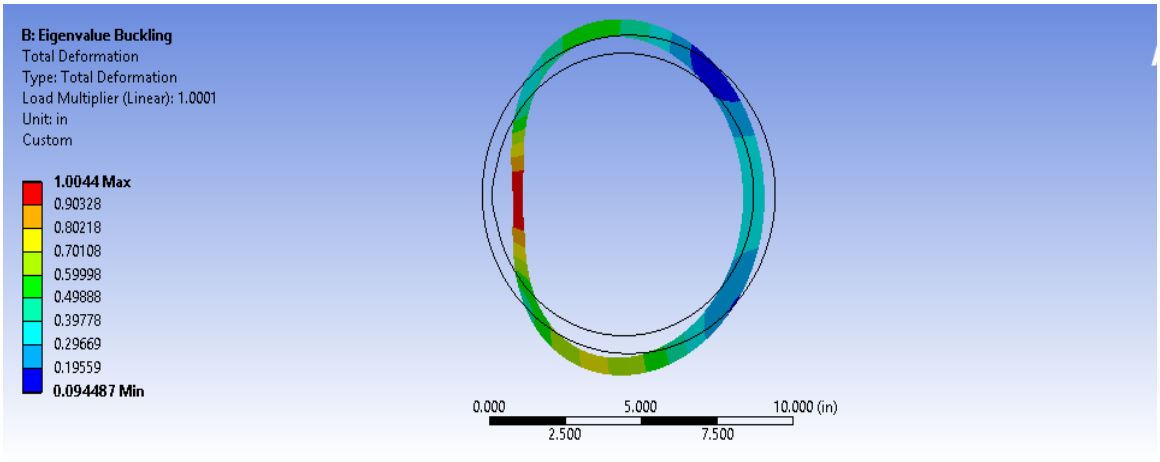

Figure 16: Deformation under Eigen buckling for 9 5/8" casing with wear as 10% of wall thickness

5 RESULTS AND DISCUSSION

5.1 Burst

In this section, the hoop stress results obtained using new proposed burst analytical model have been compared with Finite Element Analysis burst simulation results. Comparison of the analytical model results with other existing models has also been presented.

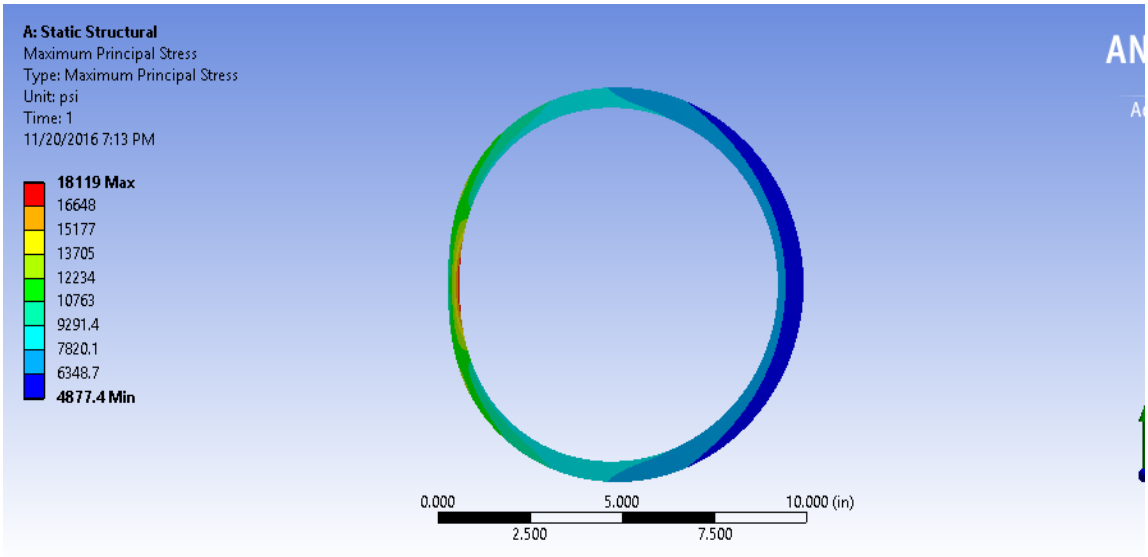

Figure 17: Hoop stress estimation for 9 5/8" casing with internal pressure of 1000 psi

5.1.1 Model Validation - Wear influence on burst pressure

As mentioned in section 2.1, API regulates the internal critical pressure in API Bulletin 5C3 [9]. The internal capacity of pipe given by Barlow's formula has a factor of 0.875 to accommodate for minimum wall thickness. Table 3 presents the comparison of the results with FEA model for 5" OD casing with wear circle radius of 1.80". To introduce the eccentricity in casing, minimum thickness (t_a) of 0.25" and maximum thickness (t_b) of 0.47" are used for calculations. The comparison has been done by varying the casing wear as a percentage of casing wall thickness from 0% to 50%. The first three columns of Table 3 contain characteristic values, such as outside diameter, nominal wall thickness and wear circle radius. The fourth column indicates the corresponding wear as a percentage of casing wall thickness varying from 10% to 50%. The fifth

column has (σ_a/P) values computed using the new proposed model (Equation 26) for non-uniform wall thickness and wear. An internal pressure of 1000 psi has been used as a loading condition in FEA model to simulate the average hoop stress at the thinnest cross section of the casing. Subsequently, to obtain the average hoop stress using the analytical model, pressure of 1000 psi is used and these values are shown in sixth column. The respective values from FEA simulation are shown in seventh column for comparison. The eight column shows the variation of the hoop stress obtained using new proposed model and the FEA model given by

$$\% \text{ Variation} = \frac{\sigma_a - \sigma_{ansys}}{\sigma_a} * 100. \tag{80}$$

Table 3: Comparison of hoop stress using analytical and numerical model - 5" OD casing

Casing Diameter	**Thickness**	**Wear circle radius**	**Wear**	$\boldsymbol{\sigma_a}$**/P Proposed model**	$\boldsymbol{\sigma_a}$	$\boldsymbol{\sigma_{FEM}}$	**Variation**
Inches	**Inches**	**Inches**	**%**	**-**	**psi**	**psi**	**%**
5	0.362	1.80	10%	10.26	10262.18	10183.31	1%
			20%	12.69	12692.30	12572.13	1%
			30%	15.79	15792.89	16311.08	3%
			40%	21.26	21262.27	19762.16	7%
			50%	32.16	32155.01	32661.80	2%

The average hoop stress values for new proposed model and FEA simulation for 5” casing with wear radius of 1.8” is presented in Table 3 are plotted in Figure 18.

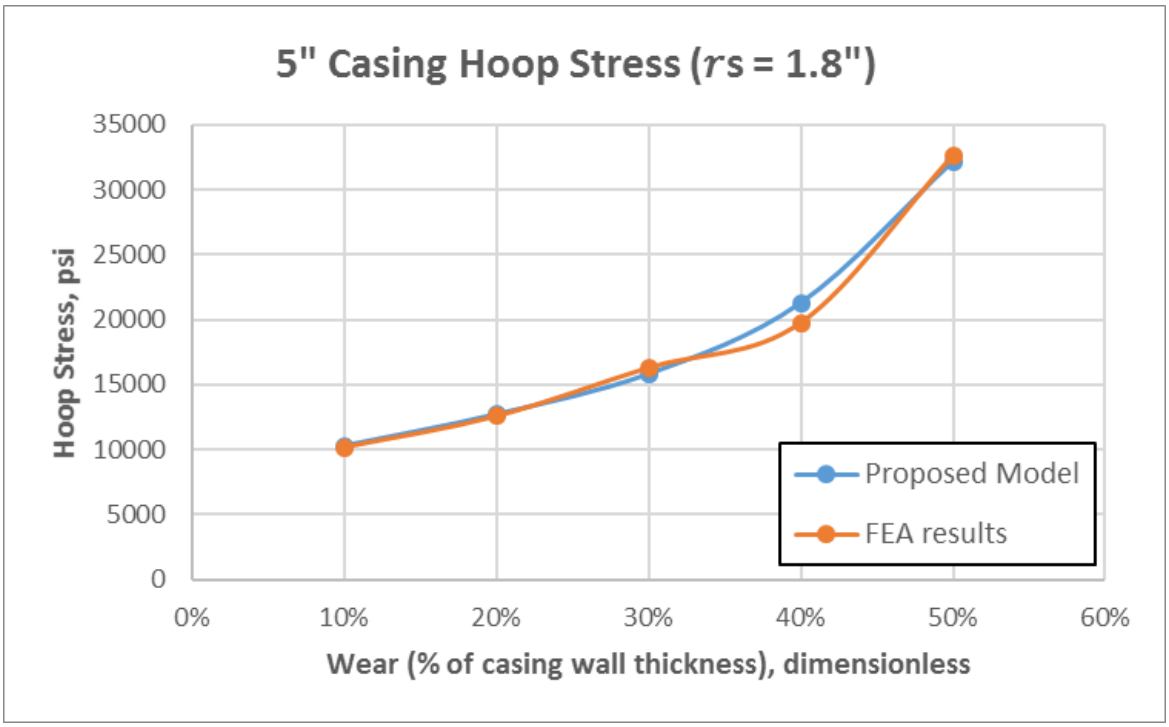

Figure 18: Plot showing comparison of hoop stress using analytical and numerical model - 5" OD casing

From Figure 18, results show a good correlation between both methods, with the deviations between 1% and 7%. From this chart it is clear that both models show that with increase in wear percentage, the average hoop stress increases. It is easy to notice very good conformity between curves formed by the new proposed model and FEM results.

Table 4 below presents the comparison of the results with FEA model for 7" OD casing with wear circle radius of 2.4". To introduce the eccentricity in casing, minimum thickness (t_a) of 0.38" and maximum thickness (t_b) of 0.70" are used for calculations. The comparison has been done by varying the casing wear as a percentage of casing wall thickness from 0% to 50%.

Table 4:Comparison of hoop stress using analytical and numerical model - 7" OD casing

Casing Diameter	Thickness	Wear circle radius	Wear	σa/P Proposed model	σa	σ_{FEM}	Variation
Inches	Inches	Inches	%	-	psi	Psi	%
7	0.540	2.40	10%	9.57	9566.42	9705.31	1%
			20%	11.88	11879.15	11592.10	2%
			30%	14.69	14694.44	14545.87	1%
			40%	19.79	19794.70	20446.10	3%
			50%	30.11	30107.08	29010.09	4%

The average hoop stress values for new proposed model and FEA simulation for 7” casing with wear radius of 2.4” is presented in Table 4 are plotted in Figure 19.

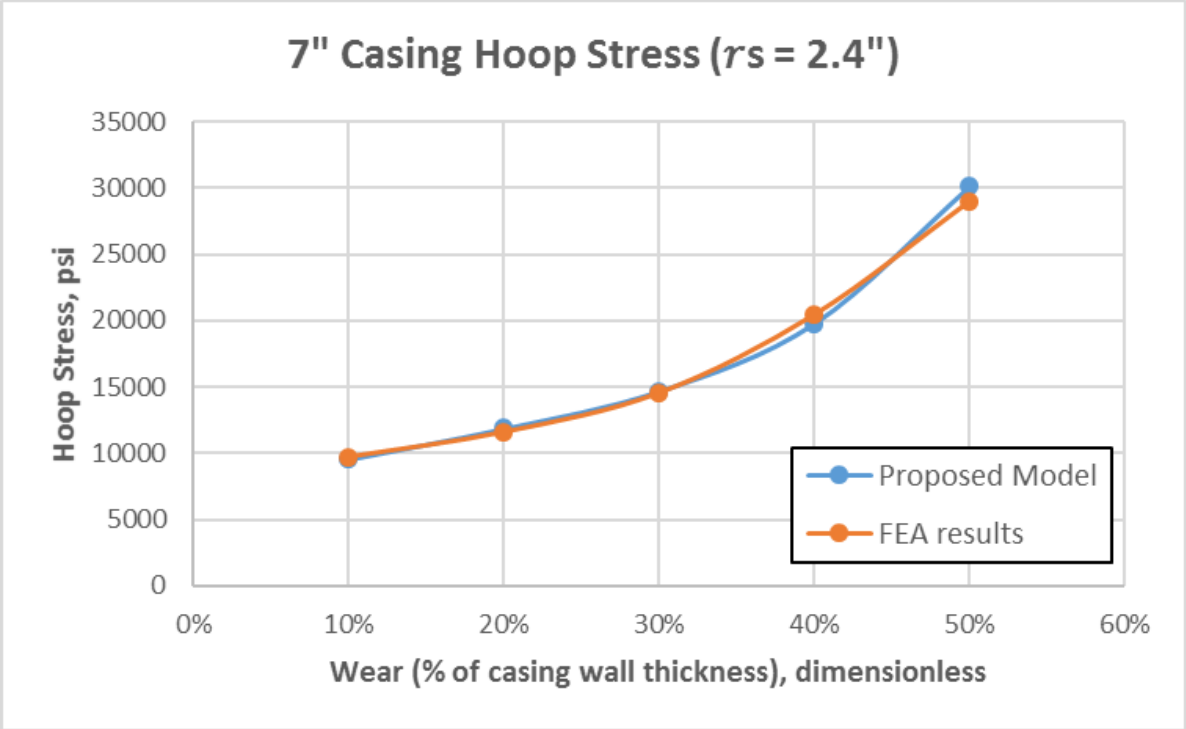

Figure 19: Plot showing comparison of hoop stress using analytical and numerical model - 7" OD casing

From Figure 19, results show a good correlation between both methods, with the deviations between 1% and 4%. From this chart it is clear that both models show that with

increase in wear percentage, the average hoop stress increases. It is easy to notice very good conformity between curves formed by the new proposed model and FEM results.

Table 5 presents the comparison of the results with FEA model for 9 5/8" OD casing with wear circle radius of 2.4". To introduce the eccentricity in casing, minimum thickness (t_a) of 0.54" and maximum thickness (t_b) of 0.70" are used for calculations. The comparison has been done by varying the casing wear as a percentage of casing wall thickness from 0% to 50%.

Table 5: Comparison of hoop stress using analytical and numerical model - 9 5/8" OD casing

Casing Diameter	**Thickness**	**Wear circle radius**	**Wear**	**σa/P Proposed model**	**σa**	σ_{FEM}	**Variation**
Inches	**Inches**	**Inches**	**%**	**-**	**psi**	**psi**	**%**
9 5/8	0.540	2.40	10%	13.71	13705.72	13476.01	2%
			20%	17.09	17087.57	16110.88	6%
			30%	20.92	20918.15	21505.72	3%
			40%	28.12	28123.53	29205.79	4%
			50%	42.57	42572.79	41285.23	3%

The average hoop stress values for new proposed model and FEA simulation for 9 5/8" casing with wear radius of 2.4" is presented in Table 5 are plotted in Figure 20.

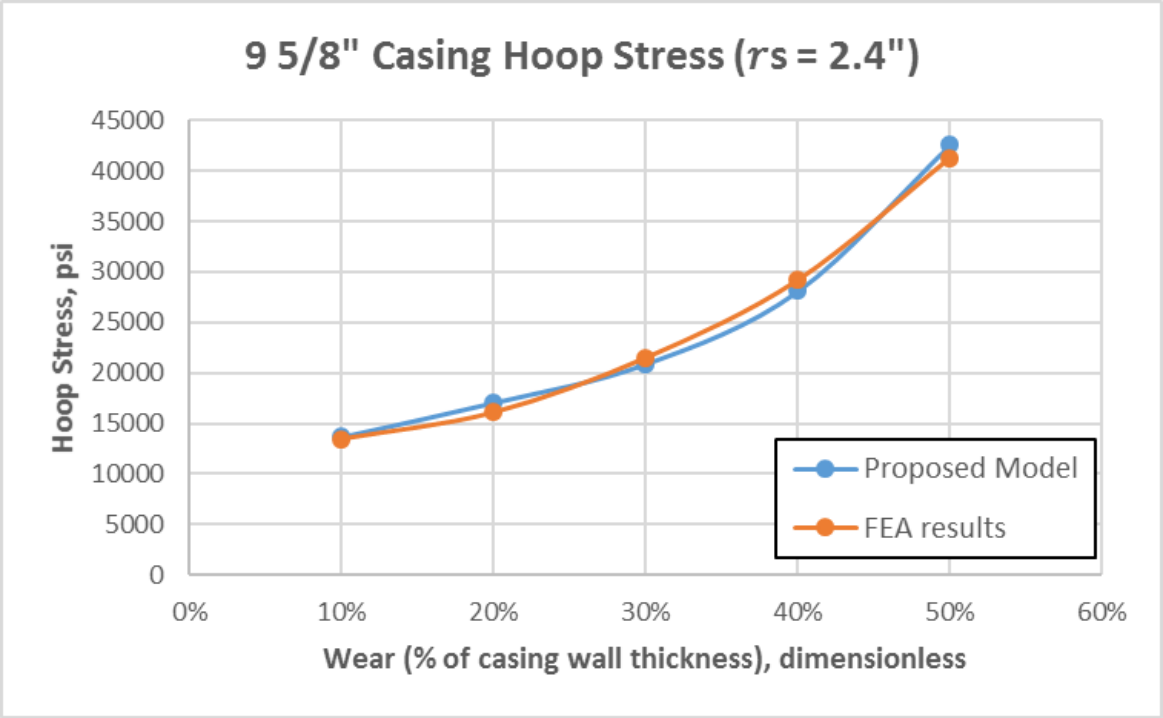

Figure 20: Plot showing comparison of hoop stress using analytical and numerical model - 9 5/8" OD casing

From Figure 20, results show a good correlation between both methods, with the deviations between 1% and 6%. From this chart it is clear that both models show that with increase in wear percentage, the average hoop stress increases. It is easy to notice very good conformity between curves formed by the new proposed model and FEM results.

Table 6 presents the comparison of the results with FEA model for 9 5/8" OD casing with wear circle radius of 3.90". To introduce the eccentricity in casing, minimum thickness (t_a) of 0.38" and maximum thickness (t_b) of 0.71" are used for calculations. The comparison has been done by varying the casing wear as a percentage of casing wall thickness from 0% to 50%.

Table 6: Comparison of hoop stress using analytical and numerical model - 9 5/8" OD casing

Casing Diameter	Thickness	Wear circle radius	Wear	σa/P Proposed model	σa	σ_{FEM}	Variation
Inches	Inches	Inches	%	-	psi	psi	%
9 5/8	0.545	3.90	10%	13.44	13439.02	13728.18	2%
			20%	16.24	16237.71	15991.35	2%
			30%	20.48	20480.58	20352.16	1%
			40%	27.58	27582.75	27977.11	1%
			50%	41.64	41639.82	39899.57	4%

The average hoop stress values for new proposed model and FEA simulation for 9 5/8" casing with wear radius of 3.90" is presented in Table 6 are plotted in Figure 21.

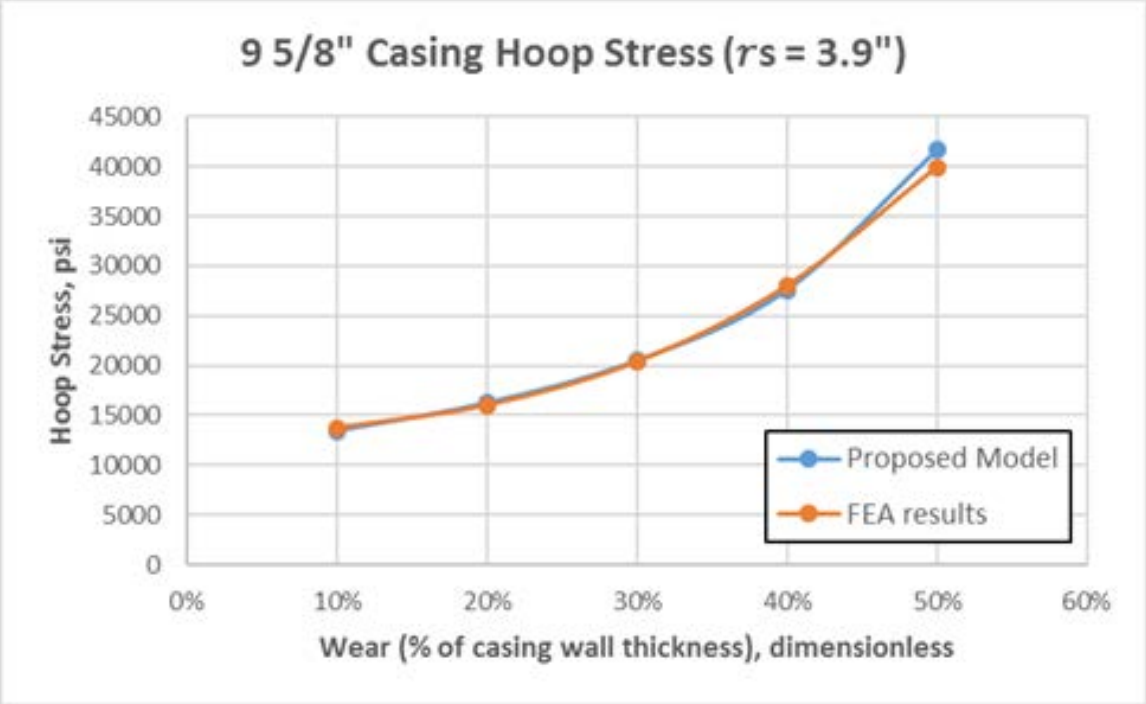

Figure 21: Plot showing comparison of hoop stress using analytical and numerical model - 9 5/8" OD casing

From Figure 21, results show a good correlation between both methods, with the deviations between 1% and 4%. From this chart it is clear that both models show that with

increase in wear percentage, the average hoop stress increases. It is easy to notice very good conformity between curves formed by the new proposed model and FEM results.

Table 7 presents the comparison of the results with FEA model for 13 3/8" OD casing with wear circle radius of 4.56". To introduce the eccentricity in casing, minimum thickness (t_a) of 0.36" and maximum thickness (t_b) of 0.67" are used for calculations. The comparison has been done by varying the casing wear as a percentage of casing wall thickness from 0% to 50%.

Table 7: Comparison of hoop stress using analytical and numerical model - 13 3/8" OD casing

Casing Diameter	Thickness	Wear circle radius	Wear	σa/P Proposed model	σa	σ_{FEM}	Variation
Inches	Inches	Inches	%	-	psi	psi	%
13 3/8	0.514	4.56	10%	20.51	20510.01	19368.75	6%
			20%	25.25	25252.45	24233.56	4%
			30%	31.13	31129.03	30763.55	1%
			40%	41.68	41679.47	41126.18	1%
			50%	62.94	62944.51	59573.74	5%

The average hoop stress values for new proposed model and FEA simulation for 13 3/8" casing with wear radius of 4.56" is presented in Table 7 are plotted in Figure 22. Results show a good correlation between both methods, with the deviations between 1% and 6%. From this chart it is clear that both models show that with increase in wear percentage, the average hoop stress increases. It is easy to notice very good conformity between curves formed by the new proposed model and FEM results.

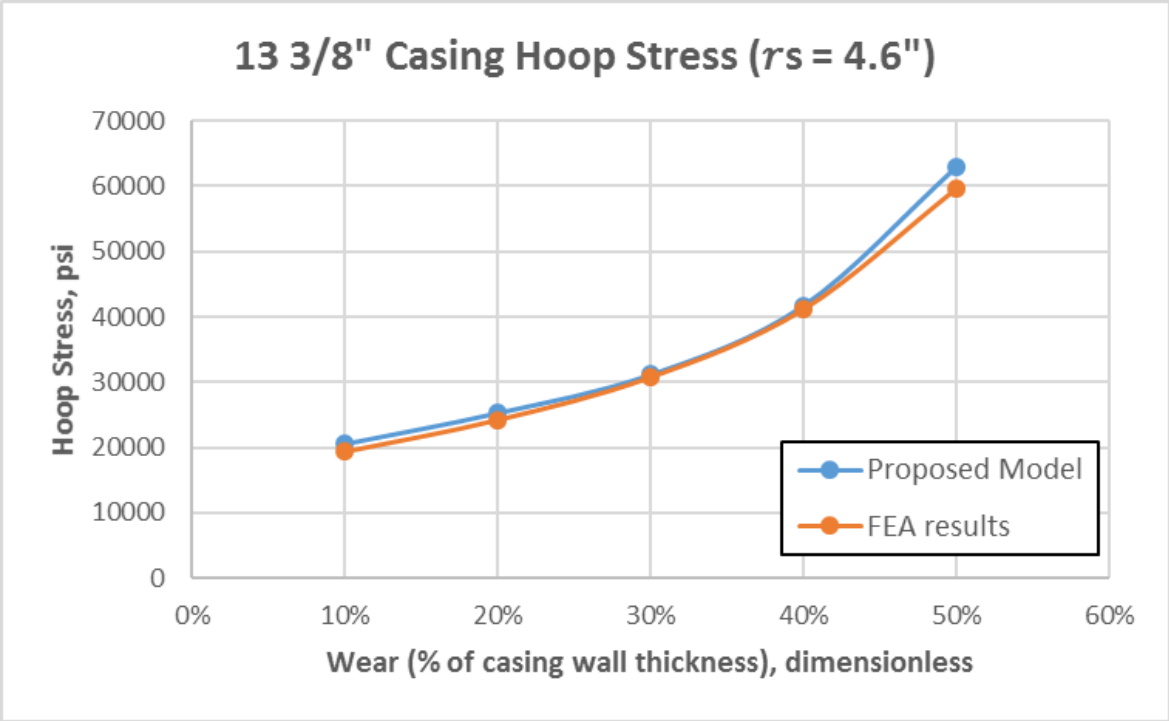

Figure 22: Plot showing comparison of hoop stress using analytical and numerical model - 13 3/8" OD casing

5.1.2 Comparison with other models

Table 8 presents the comparison of the results with existing models for 5" OD casing with wear circle radius of 1.80". To introduce the eccentricity in casing, minimum thickness (t_a) of 0.25" and maximum thickness (t_b) of 0.47" are used for calculations. The comparison has been done by varying the casing wear as a percentage of casing wall thickness from 0% to 50%. The first three columns of Table 8 contain characteristic values, such as outside diameter, nominal wall thickness and wear circle radius. The fourth column indicates the corresponding wear as a percentage of casing wall thickness varying from 10% to 50%. The fifth column has values computed by using the API equation (Equation 1). As these values consider the safety factor for minimum wall, for comparison purposes it was omitted. The sixth and seventh columns present the burst limit pressure values obtained using Nadai's (Equation 2) and Crescent – shape wear models (Equation 3) respectively. The eighth column shows the values obtained using new proposed model,

assuming constant casing wall thickness (t_a = t_b). The ninth column shows the internal burst pressure capacity values obtained using the new proposed model with non-uniform wall thickness and wear (Equation 26).

Table 8: Comparison of models for internal pressure capacity - 5" OD casing

Casing Diameter	Thickness	Wear circle radius	Wear	P API	P Nadai	P (Li and Samuel)	P (constant t)	P (Varying t)
Inches	Inches	Inches	%	psi	psi	psi	psi	psi
5	0.362	1.80	10%	14335.61	17735.94	16557.84	16605.20	10718.97
			20%	12742.80	15638.52	14539.73	14577.11	8666.67
			30%	11149.80	13574.92	12569.29	12592.43	6965.16
			40%	9557.19	11544.81	10645.74	10668.99	5173.48
			50%	7964.40	9546.42	8766.94	8791.91	3420.93

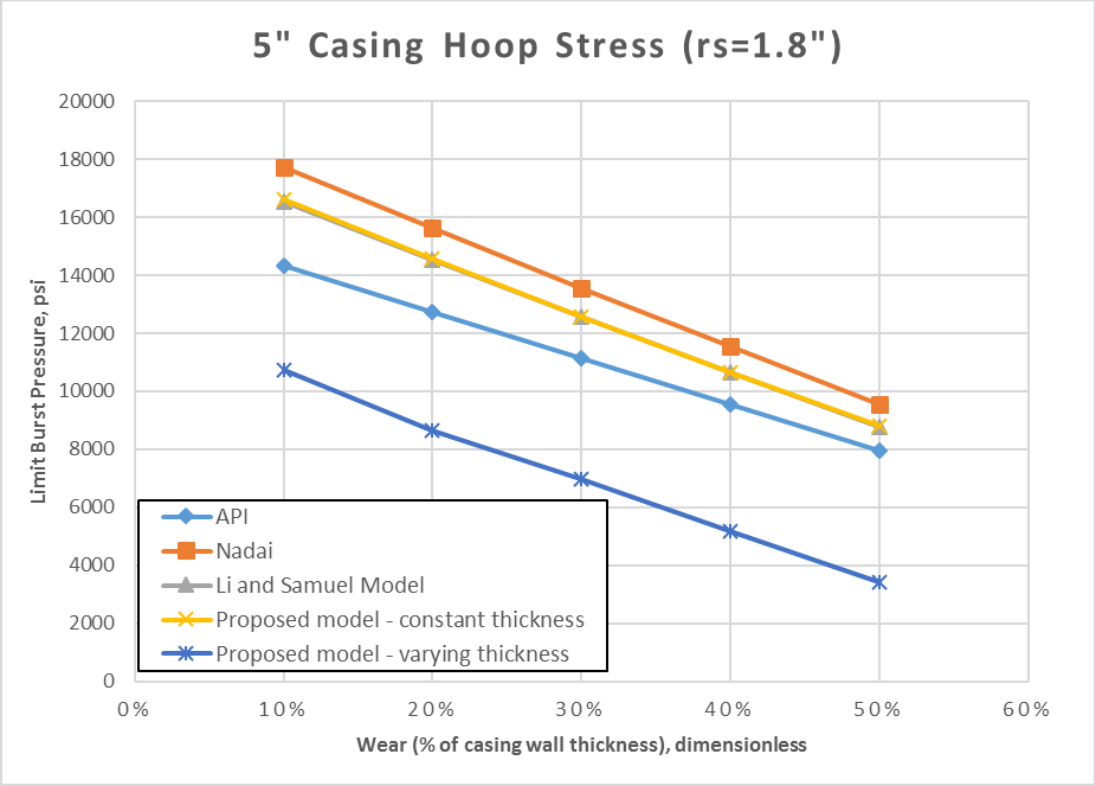

Figure 23: Plot showing comparison of models for internal pressure capacity - 5" OD casing

The average hoop stress values at the critical wear section for new proposed model and existing models for 5” casing with wear radius of 1.8” is presented in Table 8 are plotted in Figure 23.

From Figure 23, the new proposed model with constant thickness provides a higher inner pressure capacity than the API model, the pressure capacity increases with decrease in diameter. The Nadai’s model gives a higher pressure capacity compared to other models as it is based on ultimate tensile strength instead of yield strength. From this chart it is clear that all the models show that with increase in wear percentage, the limit burst pressure decreases. It is easy to notice very good conformity between curves formed by the new proposed model with constant thickness and crescent shape model. Also, the new proposed model with varying thickness has the lowest value because the lowest thickness includes the eccentricity as well.

Table 9 presents the comparison of the results with existing models for 7” OD casing with wear circle radius of 2.40”. To introduce the eccentricity in casing, minimum thickness (t_a) of 0.38” and maximum thickness (t_b) of 0.70” are used for calculations. The comparison has been done by varying the casing wear as a percentage of casing wall thickness from 0% to 50%.

Table 9: Comparison of models for internal pressure capacity - 7" OD casing

Casing Diameter	Thickness	Wear circle radius	Wear	P API	P Nadai	P (Li and Samuel)	P (constant)	P (Varying t)
Inches	Inches	Inches	%	Psi	psi	Psi	psi	psi
7	0.540	2.40	10%	15277.31	18992.45	17827.32	17841.50	11498.55
			20%	13580.25	16736.96	15640.75	15648.56	9259.92
			30%	11882.92	14520.45	13509.50	13525.12	7485.82
			40%	10185.93	12342.40	11432.47	11441.59	5557.04
			50%	8488.71	10200.79	9407.16	9415.15	3653.63

The average hoop stress values at the critical wear section for new proposed model and existing models for 7” casing with wear radius of 2.4” is presented in Table 9 are plotted in Figure 24.

From Figure 24, the new proposed model with constant thickness provides a higher inner pressure capacity than the API model, the pressure capacity increases with decrease in diameter. The Nadai’s model gives a higher pressure capacity compared to other models. From this chart it is clear that both models show that with increase in wear percentage, the limit burst pressure decreases. It is easy to notice very good conformity between curves formed by the new proposed model with constant thickness and crescent shape model.

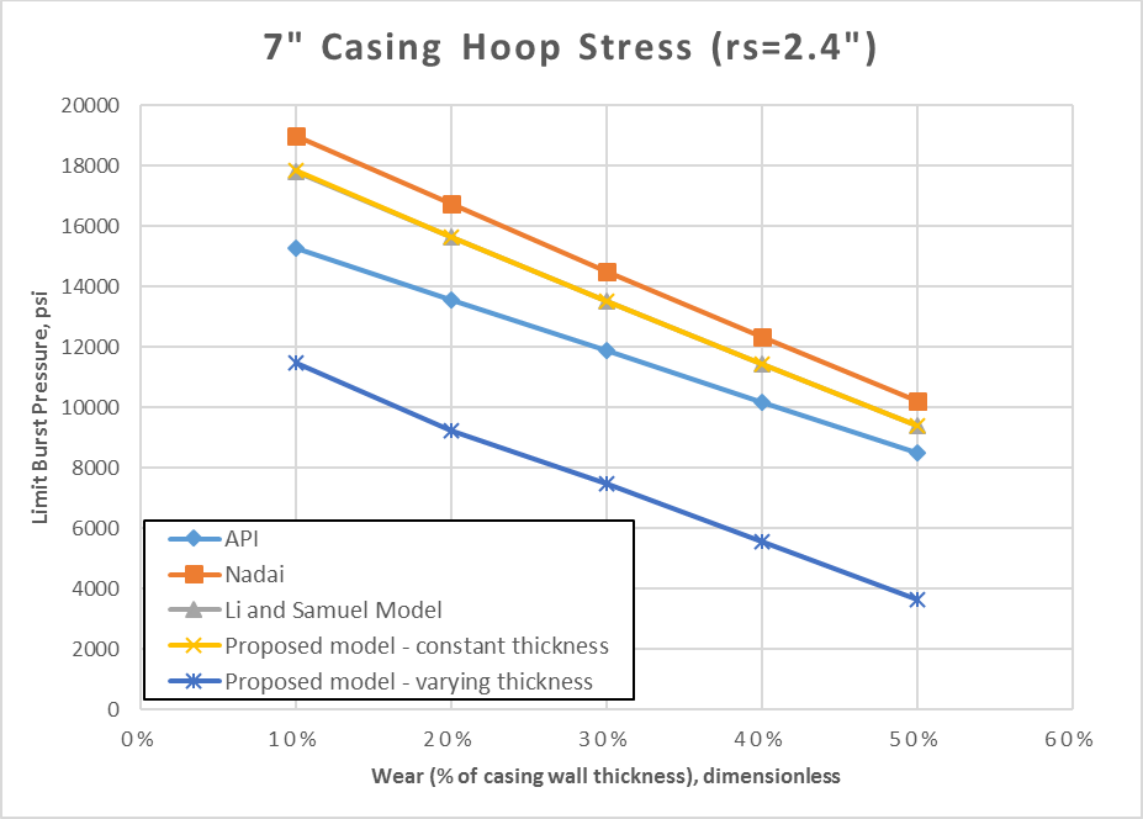

Figure 24: Plot showing comparison of models for internal pressure capacity - 7" OD casing

Table 10 presents the comparison of the results with existing models for 9 5/8” OD casing with wear circle radius of 2.40”. To introduce the eccentricity in casing, minimum thickness (t_a) of 0.38” and maximum thickness (t_b) of 0.70” are used for calculations. The comparison has been done by varying the casing wear as a percentage of casing wall thickness from 0% to 50%.

Table 10: Comparison of models for internal pressure capacity - 9 5/8" OD casing

Casing Diameter	Thickness	Wear circle radius	Wear	P API	P Nadai	P (Li and Samuel)	P (constant t)	P (Varying t)
Inches	Inches	Inches	%	psi	psi	psi	psi	psi
9 5/8	0.540	2.40	10%	11213.71	13657.99	12528.3	12400.92	8025.85
			20%	9967.98	12065.35	11033.6	10921.06	6437.43
			30%	8722.21	10493.29	9566.03	9463.52	5258.59
			40%	7476.42	8940.416	8124.99	8028.64	3911.32
			50%	6230.78	7406.488	6710.02	6643.56	2583.81

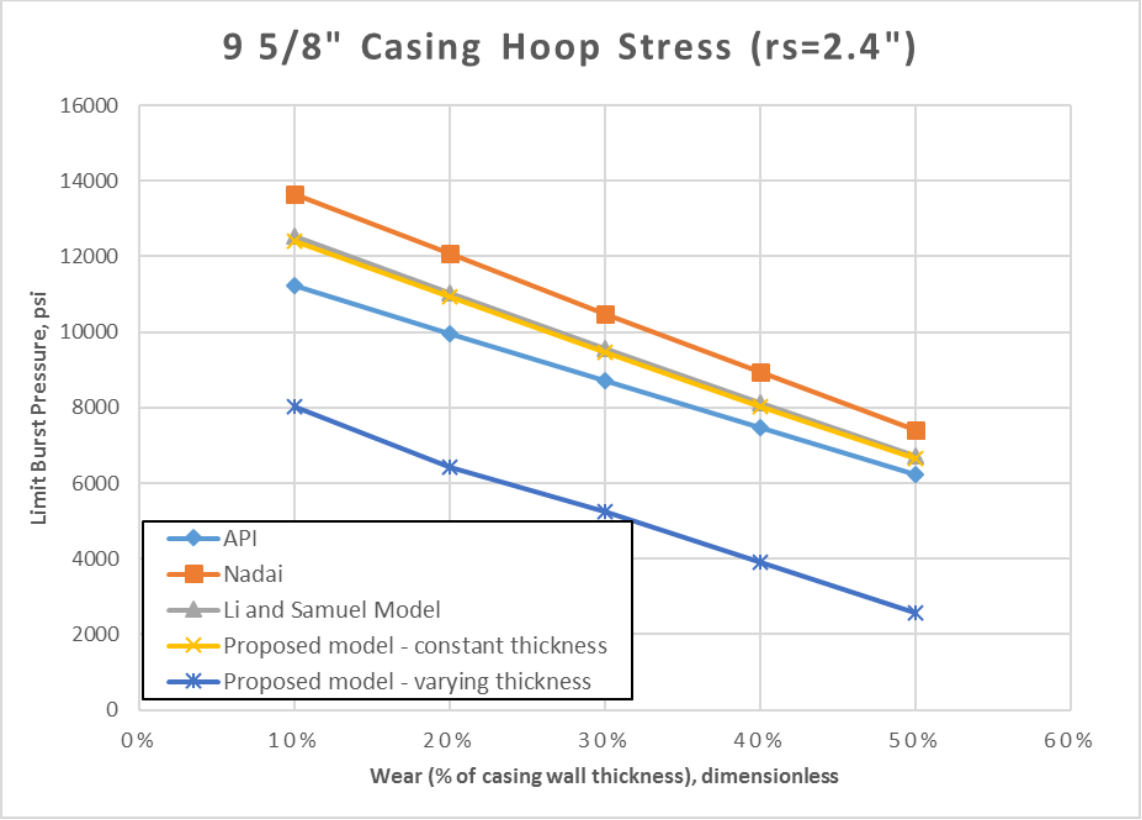

Figure 25: Plot showing comparison of models for internal pressure capacity - 9 5/8" OD casing

The average hoop stress values at the critical wear section for new proposed model and existing models for 9 5/8” casing with wear radius of 2.4” is presented in Table 10 are plotted in Figure 25.

From Figure 25, the new proposed model with constant thickness provides a higher inner pressure capacity than the API model, the pressure capacity increases with decrease in diameter. The Nadai’s model gives a higher pressure capacity compared to other models. From this chart it is clear that both models show that with increase in wear percentage, the limit burst pressure decreases. It is easy to notice very good conformity between curves formed by the new proposed model with constant thickness and crescent shape model.

Table 11: Comparison of models for internal pressure capacity – 9 5/8" OD casing

Casing Diameter	Thickness	Wear circle radius	Wear	P API	P Nadai	P (Li and Samuel)	P (constant t)	P (Varying t)
Inches	Inches	Inches	%	psi	psi	psi	psi	psi
9 5/8	0.545	3.90	10%	11211.58	13654.33	12525.71	12547.25	8185.12
			20%	9965.89	12062.70	11031.11	11037.44	6774.36
			30%	8720.06	10490.59	9563.52	9572.57	5370.94
			40%	7474.33	8937.83	8122.60	8122.41	3988.00
			50%	6228.55	7403.75	6707.51	6712.95	2641.70

Table 11 presents the comparison of the results with existing models for 9 5/8” OD casing with wear circle radius of 3.90”. To introduce the eccentricity in casing, minimum thickness (t_a) of 0.38” and maximum thickness (t_b) of 0.70” are used for calculations. The comparison has been done by varying the casing wear as a percentage of casing wall thickness from 0% to 50%.

The average hoop stress values at the critical wear section for new proposed model and existing models for 9 5/8” casing with wear radius of 3.90” is presented in Table 11 are plotted in Figure 26.

From Figure 26, the new proposed model with constant thickness provides a higher inner pressure capacity than the API model, the pressure capacity increases with decrease in diameter. The Nadai's model gives a higher pressure capacity compared to other models. From this chart it is clear that both models show that with increase in wear percentage, the limit burst pressure decreases. It is easy to notice very good conformity between curves formed by the new proposed model with constant thickness and crescent shape model.

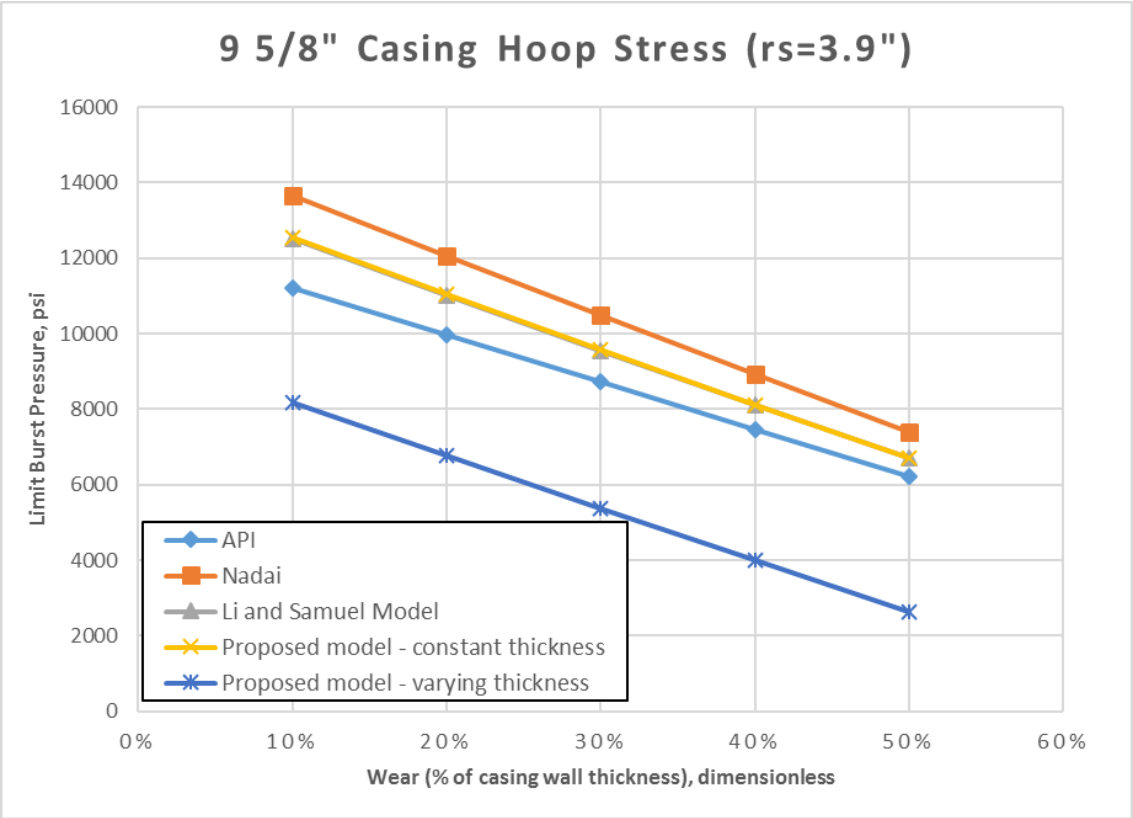

Figure 26: Plot showing comparison of models for internal pressure capacity - 9 5/8" OD casing

Table 12 presents the comparison of the results with existing models for 13 3/8" OD casing with wear circle radius of 4.56". To introduce the eccentricity in casing, minimum thickness (t_a) of 0.36" and maximum thickness (t_b) of 0.67" are used for calculations. The comparison has been done by varying the casing wear as a percentage of casing wall thickness from 0% to 50%.

Table 12: Comparison of models for internal pressure capacity – 13 3/8" OD casing

Casing Diameter	Thickness	Wear circle radius	Wear	P API	P Nadai	P (Li and Samuel)	P (constant t)	P (Varying t)
Inches	Inches	Inches	%	psi	psi	psi	psi	psi
13 3/8	0.514	4.56	10%	7609.19	9105.02	8192.22	8183.44	5363.23
			20%	6763.75	8060.55	7237.59	7237.62	4356.01
			30%	5918.22	7024.48	6294.38	6286.92	3533.68
			40%	5072.82	5996.95	5362.65	5359.72	2639.19
			50%	4227.23	4977.45	4441.87	4437.26	1747.57

The average hoop stress values at the critical wear section for new proposed model and existing models for 13 3/8” casing with wear radius of 4.56” is presented in Table 12 are plotted in Figure 27.

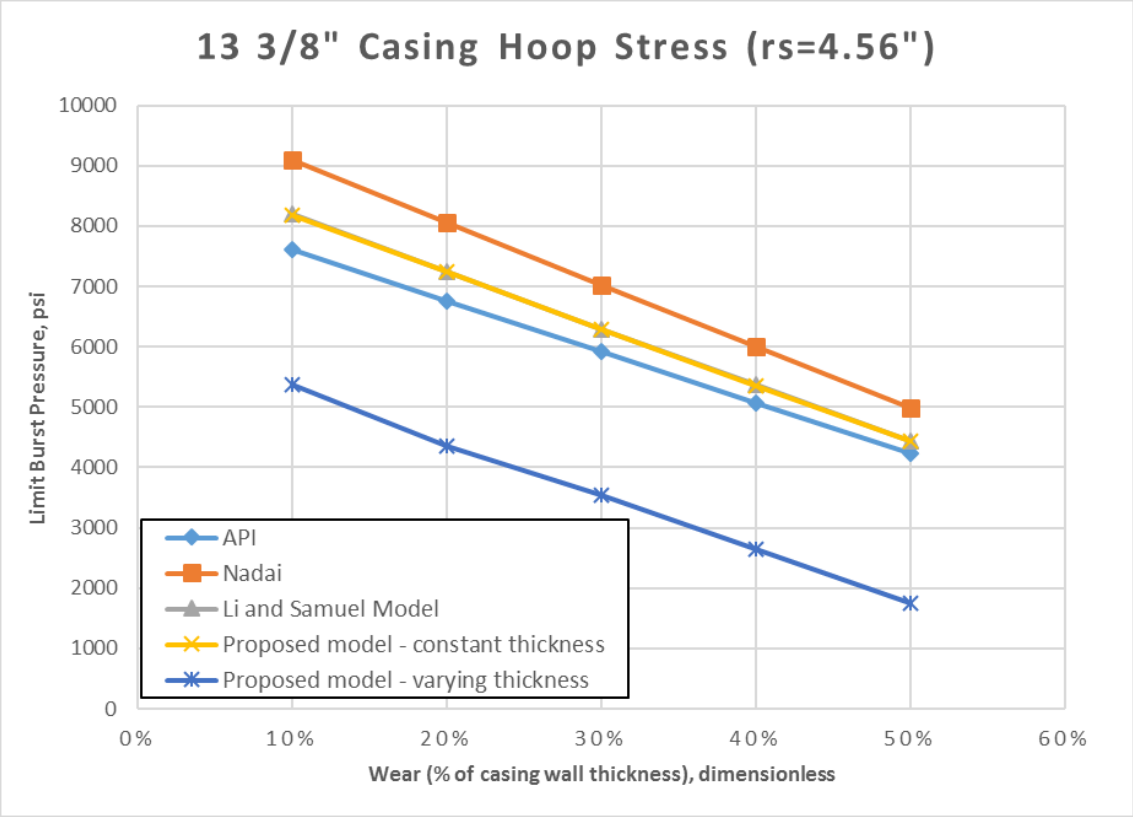

Figure 27: Plot showing comparison of models for internal pressure capacity - 13 3/8" OD casing

From Figure 27, the new proposed model with constant thickness provides a higher inner pressure capacity than the API model, the pressure capacity increases with decrease in diameter. The Nadai's model gives a higher pressure capacity compared to other models. From this chart it is clear that both models show that with increase in wear percentage, the limit burst pressure decreases. It is easy to notice very good conformity between curves formed by the new proposed model with constant thickness and crescent shape model.

5.1.3 Non-uniformity influence on burst pressure

In this section, limit burst pressure calculations have been done by varying the thickness of the casing in the bent cross section. Casing wear has not been considered in these calculations. The maximum thickness has been varied from 100% to 130% in the increments of 5%. Similarly, the minimum thickness has been varied from 70% to 100% in the increments of 5%.

Table 13, Table 14, Table 15 and Table 16 presents the calculations of limit burst pressure with varying thickness for 5", 7", 9 5/8" and 13 3/8" OD casings respectively. The first two columns of tables contain characteristic values, such as outside diameter and nominal wall thickness. The third column indicates the corresponding thickness variation as a percentage of casing wall thickness varying from 5% to 30%. The fifth and sixth columns have (σ_a/P) and (σ_b/P) values computed using the new proposed model (Equation 12) for non-uniform wall thickness without wear. The eight column shows the calculated limit burst pressure capacity at the corresponding varied thickness using new proposed model.

Table 13: Burst pressure capacity with varying thickness - 5" OD casing

Casing Diameter	Thickness	Thickness reduction	ta	tb	σa/P	σb/P	P
Inches	Inches	%	psi	psi	psi	psi	psi
5	0.362	30%	0.25	0.47	8.44	4.54	13037.42
		25%	0.27	0.45	7.87	4.72	13968.66
		20%	0.29	0.43	7.38	4.92	14899.91
		15%	0.31	0.42	6.95	5.14	15831.15
		10%	0.33	0.40	6.56	5.37	16762.39
		5%	0.34	0.38	6.22	5.62	17693.64
		0%	0.36	0.36	5.91	5.91	18624.88

Table 14: Burst pressure capacity with varying thickness - 7" OD casing

Casing Diameter	Thickness	Thickness reduction	ta	tb	σa/P	σb/P	P
Inches	Inches	%	psi	psi	psi	psi	psi
7	0.540	30%	0.38	0.70	7.83	4.22	14047.30
		25%	0.41	0.68	7.31	4.39	15050.68
		20%	0.43	0.65	6.85	4.57	16054.05
		15%	0.46	0.62	6.45	4.77	17057.43
		10%	0.49	0.59	6.09	4.98	18060.81
		5%	0.51	0.57	5.77	5.22	19064.19
		0%	0.54	0.54	5.48	5.48	20067.57

Table 15: Burst pressure capacity with varying thickness - 9 5/8" OD casing

Casing Diameter	Thickness	Thickness reduction	ta	tb	σa/P	σb/P	P
Inches	Inches	%	psi	psi	psi	psi	psi
9 5/8	0.545	30%	0.38	0.71	11.19	6.02	9833.63
		25%	0.41	0.68	10.44	6.26	10536.03
		20%	0.44	0.65	9.79	6.53	11238.43
		15%	0.46	0.63	9.21	6.81	11940.83
		10%	0.49	0.60	8.70	7.12	12643.23
		5%	0.52	0.57	8.24	7.46	13345.64
		0%	0.55	0.55	7.83	7.83	14048.04

Table 16: Burst pressure capacity with varying thickness - 13 3/8" OD casing

Casing Diameter	Thickness	Thickness reduction	ta	tb	σa/P	σb/P	P
Inches	Inches	%	psi	psi	psi	psi	psi
13 3/8	0.514	30%	0.36	0.67	17.16	9.24	6410.95
		25%	0.39	0.64	16.01	9.61	6868.88
		20%	0.41	0.62	15.01	10.01	7326.80
		15%	0.44	0.59	14.13	10.44	7784.73
		10%	0.46	0.57	13.35	10.92	8242.65
		5%	0.49	0.54	12.64	11.44	8700.58
		0%	0.51	0.51	12.01	12.01	9158.50

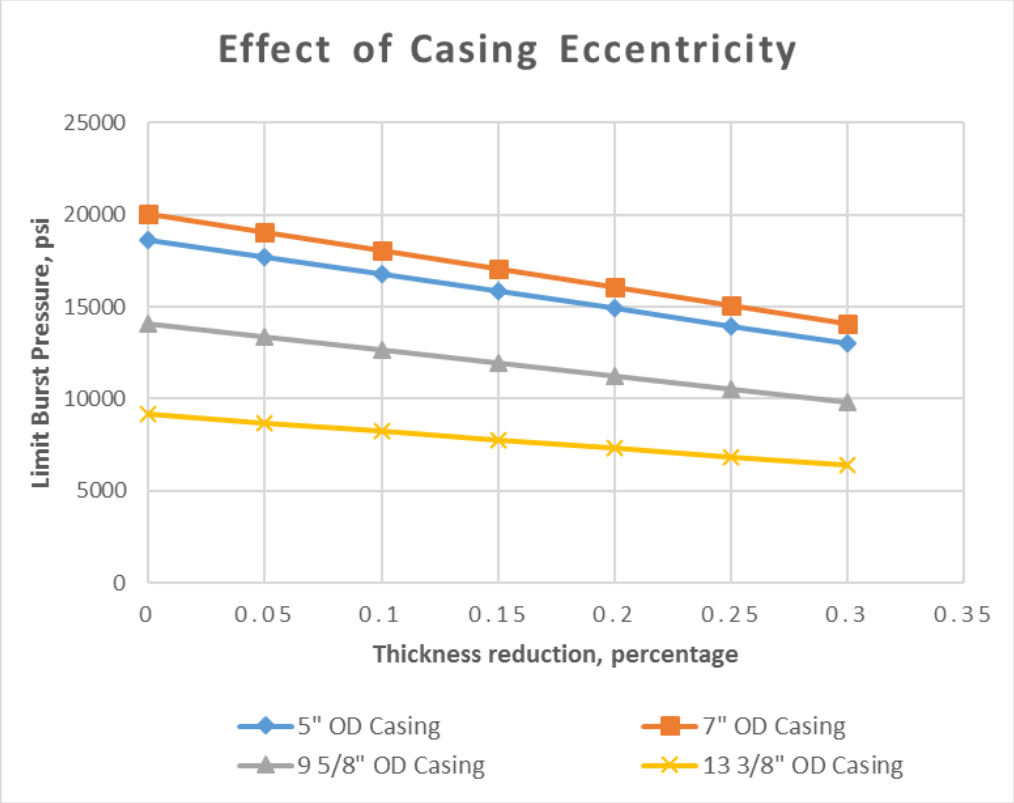

Figure 28: Plot showing burst pressure capacity with varying thickness for standard casing sizes

Figure 28 shows the variation of inner pressure capacity of casing with change in thickness percentage variation. As expected, as the percentage increase of thickness increases, burst pressure capacity decreases. As the casing size increases, the burst pressure capacity even further decreases.

5.1.4 Case Studies

Four case studies are presented to emphasize the difference between the new analytical model and existing API model while attempting to estimate the strength degradation factors based on wear percentage and wear radius. Four worn casings with different geometrical configurations were designed to compare casing burst and elastic collapse pressure predictions using the newly proposed models. The geometrical information is listed in Table 2. The casing in Case 2, 3 and 4 had a similar thickness but different nominal radius. The casing in Case 3 and 4 had the same geometrical configuration but a different wear part radius to research the influence of the wear part circle radius.

5.1.4.1 Case 1

This case compares the values of casing burst strength of a 5” casing obtained using newly proposed model versus the API model. As the analysis is done for the casing with varying thickness, the maximum thickness is considered to be 0.70” and minimum thickness to be 0.38”. The comparison has been done varying the casing wear as a percentage of casing wall thickness from 0% to 50%. The comparison in Table clearly shows that the API model underestimates the burst strength compared to the proposed model. Casing with less wear has the maximum variation of burst rating and gradually decreases with increasing wear.

Table 17: Case 1 - 5" OD Casing comparison

Casing Diameter	Thickness	Wear circle radius	Wear	P API	P (New Model)	Variation
Inches	Inches	Inches	%	psi	psi	%
5	0.362	1.80	10%	9556.80	10718.97	12%
			20%	7964.00	8666.67	9%
			30%	6371.20	6965.16	9%
			40%	4778.40	5173.48	8%
			50%	3185.60	3420.93	7%

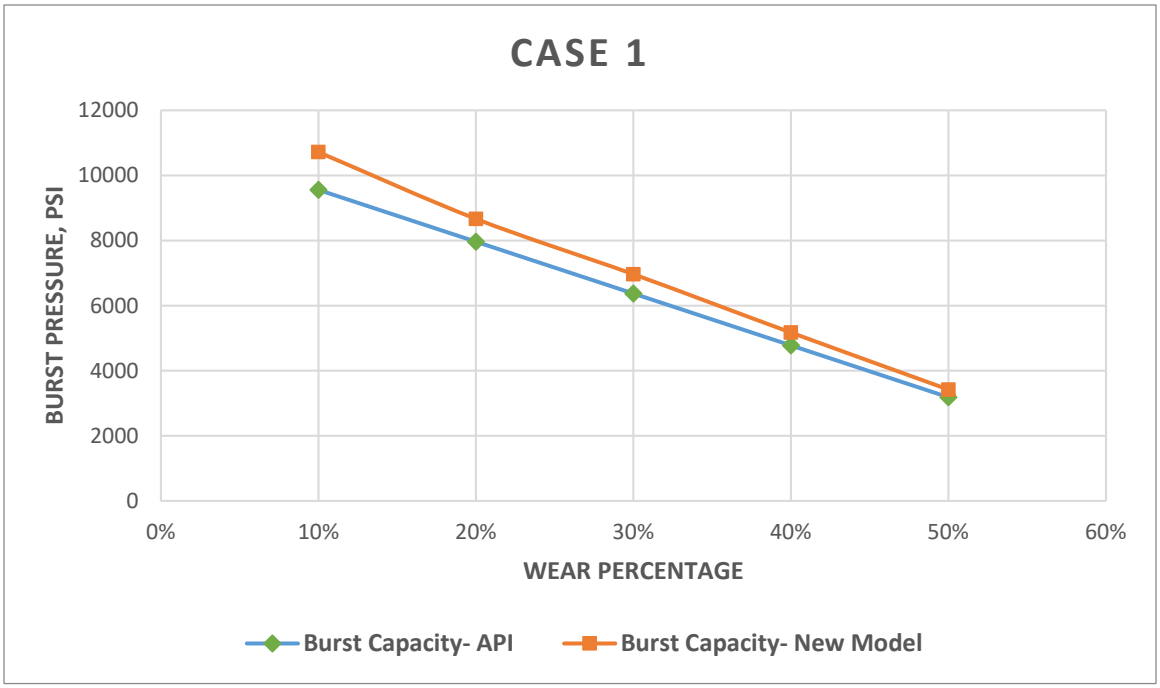

Figure 29: Case 1 - 5" OD Casing comparison

5.1.4.2 Case 2

This case is similar to the previous study which compares the values of casing burst strength of a 7 “casing obtained using newly proposed model versus the API model. The maximum thickness is considered to be 0.70” and minimum thickness to be 0.38”. The comparison has been done varying the casing wear as a percentage of casing wall thickness from 0% to 50%. The maximum variation of the burst pressure obtained using the new model is 13 % of the API burst pressure.

Table 18: Case 2 - 7" OD Casing comparison

Casing Diameter	Thickness	Wear circle radius	Wear	P API	P (New Model)	Variation
Inches	Inches	Inches	%	psi	psi	%
7	0.540	2.40	10%	10182.86	11498.55	13%
			20%	8485.71	9259.92	9%
			30%	6788.57	7485.82	10%
			40%	5091.43	5557.04	9%
			50%	3394.29	3653.63	8%

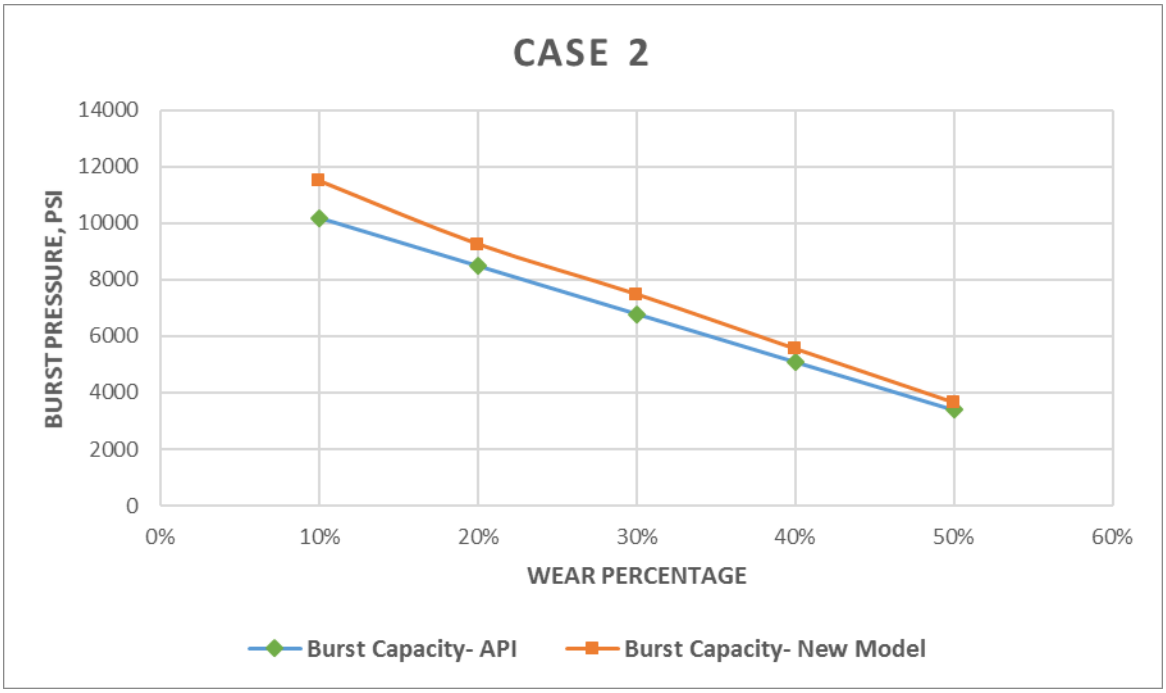

Figure 30: Case 2 - 7" OD Casing comparison

5.1.4.3 Case 3

This case compares the values of casing burst strength of a 9 5/8 “casing obtained using newly proposed model versus the API model. As the analysis is done for the casing with varying thickness, the maximum thickness is considered to be 0.70” and minimum thickness to be 0.38”. The comparison has been done varying the casing wear as a percentage of casing wall thickness from 0% to 50%.

Table 19: Case 3 - 9 5/8" OD Casing comparison

Casing Diameter	Thickness	Wear circle radius	Wear	P API	P (New Model)	Variation
Inches	Inches	Inches	%	psi	psi	%
9 5/8	0.540	2.40	10%	7405.71	8025.85	8%
			20%	6171.43	6437.43	4%
			30%	4937.14	5258.59	7%
			40%	3702.86	3911.32	6%
			50%	2468.57	2583.81	5%

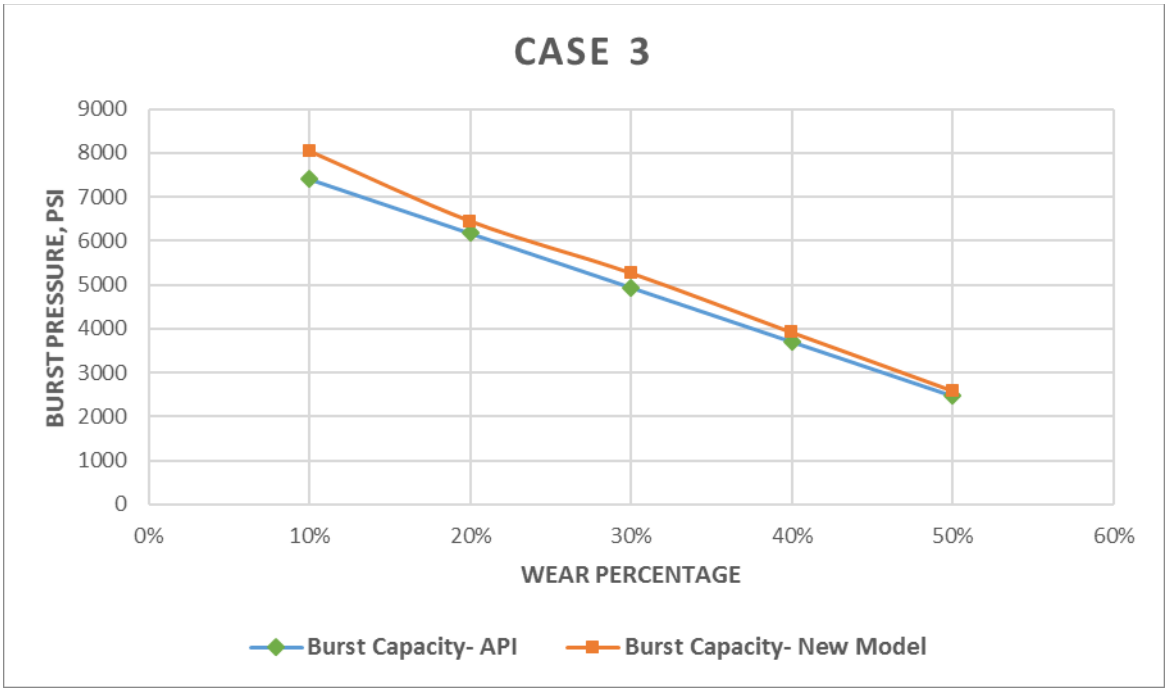

Figure 31:Case 3 - 9 5/8" OD Casing comparison

5.1.4.4 Case 4

This case is similar to the previous study which compares the values of casing burst strength of a 9 5/8 "casing obtained using newly proposed model versus the API model. The minimum thickness is taken 75% of the nominal thickness which is 0.38" and maximum thickness to be 0.70". For this case study the wear radius has been changed to 3.9".

Table 20: Case 4 - 9 5/8" OD Casing comparison

Casing Diameter	Thickness	Wear circle radius	Wear	P API	P (New Model)	Variation
Inches	Inches	Inches	%	psi	psi	%
9 5/8	0.540	3.90	10%	7474.29	8025.85	7%
			20%	6228.57	6437.43	3%
			30%	4982.86	5258.59	6%
			40%	3737.14	3911.32	5%
			50%	2491.43	2583.81	4%

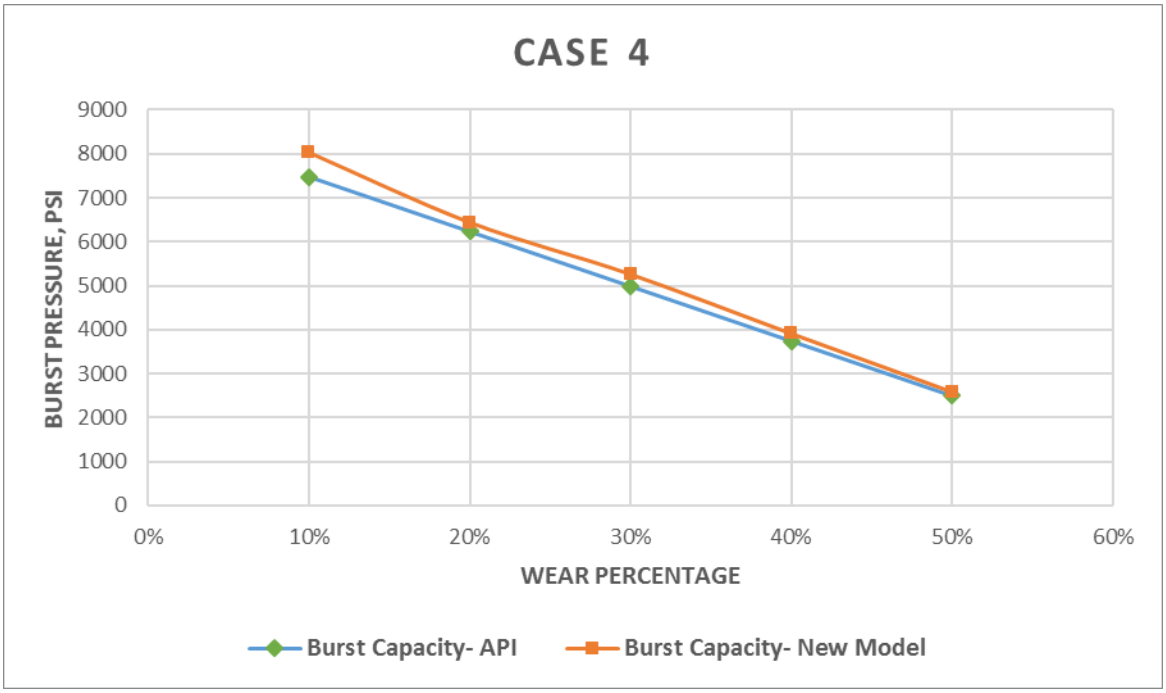

Figure 32: Case 4 - 9 5/8" OD Casing comparison

5.1.4.5 Case 5

This case is similar to the previous study which compares the values of casing burst strength of a 13 3/8 "casing obtained using newly proposed model versus the API model. As the analysis is done for the casing with varying thickness, the maximum thickness is considered to be 0.36" and minimum thickness to be 0.67". As the casing size increases, the variation of the pressure with API decreases gradually.

Table 21: Case 5 - 13 3/8" OD Casing comparison

Casing Diameter	Thickness	Wear circle radius	Wear	P API	P (New Model)	Variation
Inches	Inches	Inches	%	psi	psi	%
13 3/8	0.540	4.56	10%	5072.75	5363.23	6%
			20%	4227.29	4356.01	3%
			30%	3381.83	3533.68	4%
			40%	2536.37	2639.19	4%
			50%	1690.92	1747.57	3%

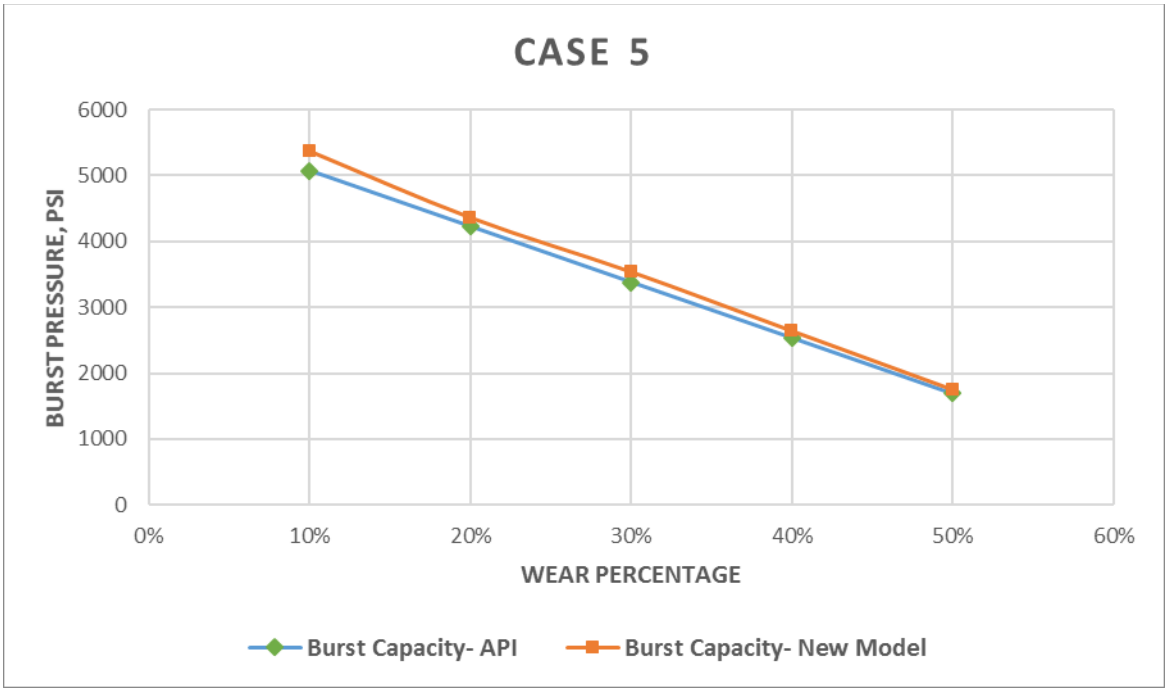

Figure 33: Case 5 - 13 3/8" OD Casing comparison

5.2 Bending

In this section, limit bending moment calculations have been done using the new proposed model for casing with varying thickness and wear. As mentioned in Section 2.4, with casing wear and non-uniform thickness, the neutral axis would shift away from the central axis. Firstly, the new position of the neutral axis has been calculated from the angles β and β'. The second moment of inertia (I) is calculated using β and β'. Bending moment capacities (*M*) are determined by using the corresponding I values. Bending moment capacities of all the commercial casing sizes have been calculated as shown by varying the wear percentages.

The comparison has been done by varying the casing wear as a percentage of casing wall thickness from 0% to 50%. The first three columns of Table 22 contain characteristic values, such as outside diameter, nominal wall thickness and wear circle radius. The fourth column indicates the corresponding wear as a percentage of casing wall thickness varying from 10% to 50%. The

fifth and sixth columns have β, β' values computed using the new proposed model (Equation 59) for non-uniform wall thickness and wear. Based on the calculated new neutral axis position, second moment of inertia (*I*) values have been calculated and shown in seventh column. The eighth and ninth columns have the values of bending moment capacity and variation of the bending moment from 0 % to 50% wear obtained using new proposed model.

Table 22: Bending moment capacity with wear - 5" OD casing

Casing Diameter	Thickness	Wear circle radius	Wear	β	β'	I	M	Maximum Variation
Inches	Inches	Inches	%	degrees	degrees	in^4	in-kips	%
5	0.362	1.80	0%	72.0	68.5	58.36	2284.99	17.60%
			10%	70.6	66.8	56.97	2212.83	
			20%	69.2	65.1	55.46	2136.32	
			30%	67.7	63.2	53.82	2055.69	
			40%	66.1	61.3	52.05	1971.17	
			50%	64.6	59.2	50.15	1882.94	

Table 23: Bending moment capacity with wear - 5" OD casing

Casing Diameter	Thickness	Wear circle radius	Wear	β	β'	I	M	Maximum Variation
Inches	Inches	Inches	%	degrees	degrees	in^4	in-kips	%
7	0.540	2.40	0%	73.2	69.8	221.43	6428.27	17.64%
			10%	71.8	68.0	215.68	6222.90	
			20%	70.3	66.2	209.48	6006.31	
			30%	68.8	64.3	202.84	5779.06	
			40%	67.3	62.3	195.77	5541.67	
			50%	65.7	60.3	188.25	5294.59	

Table 24:Bending moment capacity with wear - 9 5/8" OD casing

Casing Diameter	Thickness	Wear circle radius	Wear	β	β'	I	M	Maximum Variation
Inches	Inches	Inches	%	degrees	degrees	in^4	in-kips	%
9 5/8	0.540	2.40	0%	82.6	81.6	880.77	19608.48	1.41%
			10%	82.5	81.5	878.92	19557.22	
			20%	82.3	81.3	876.98	19504.09	
			30%	82.2	81.1	874.97	19449.04	
			40%	82.0	81.0	872.87	19391.99	
			50%	81.9	80.8	870.69	19332.90	

Table 25: Bending moment capacity with wear - 9 5/8" OD casing

Casing Diameter	Thickness	Wear circle radius	Wear	β	β'	I	M	Maximum Variation
Inches	Inches	Inches	%	degrees	degrees	in^4	in-kips	%
9 5/8	0.540	3.90	0%	86.3	85.9	898.52	20268.93	19.40%
			10%	77.5	75.8	825.38	18053.71	
			20%	76.1	74.2	809.43	17622.35	
			30%	74.8	72.7	793.36	17196.58	
			40%	73.5	71.2	776.94	16769.40	
			50%	72.2	69.7	760.04	16337.10	

Table 26: Bending moment capacity with wear - 13 3/8" OD casing

Casing Diameter	Thickness	Wear circle radius	Wear	β	β'	I	M	Maximum Variation
Inches	Inches	Inches	%	degrees	degrees	in^4	in-kips	%
13 3/8	0.514	4.56	0%	82.3	81.6	3198.42	51571.85	1.53%
			10%	82.1	81.4	3190.61	51421.90	
			20%	81.9	81.2	3182.56	51268.04	
			30%	81.7	81.0	3174.28	51110.21	
			40%	81.5	80.8	3165.75	50948.31	
			50%	81.3	80.6	3156.98	50782.28	

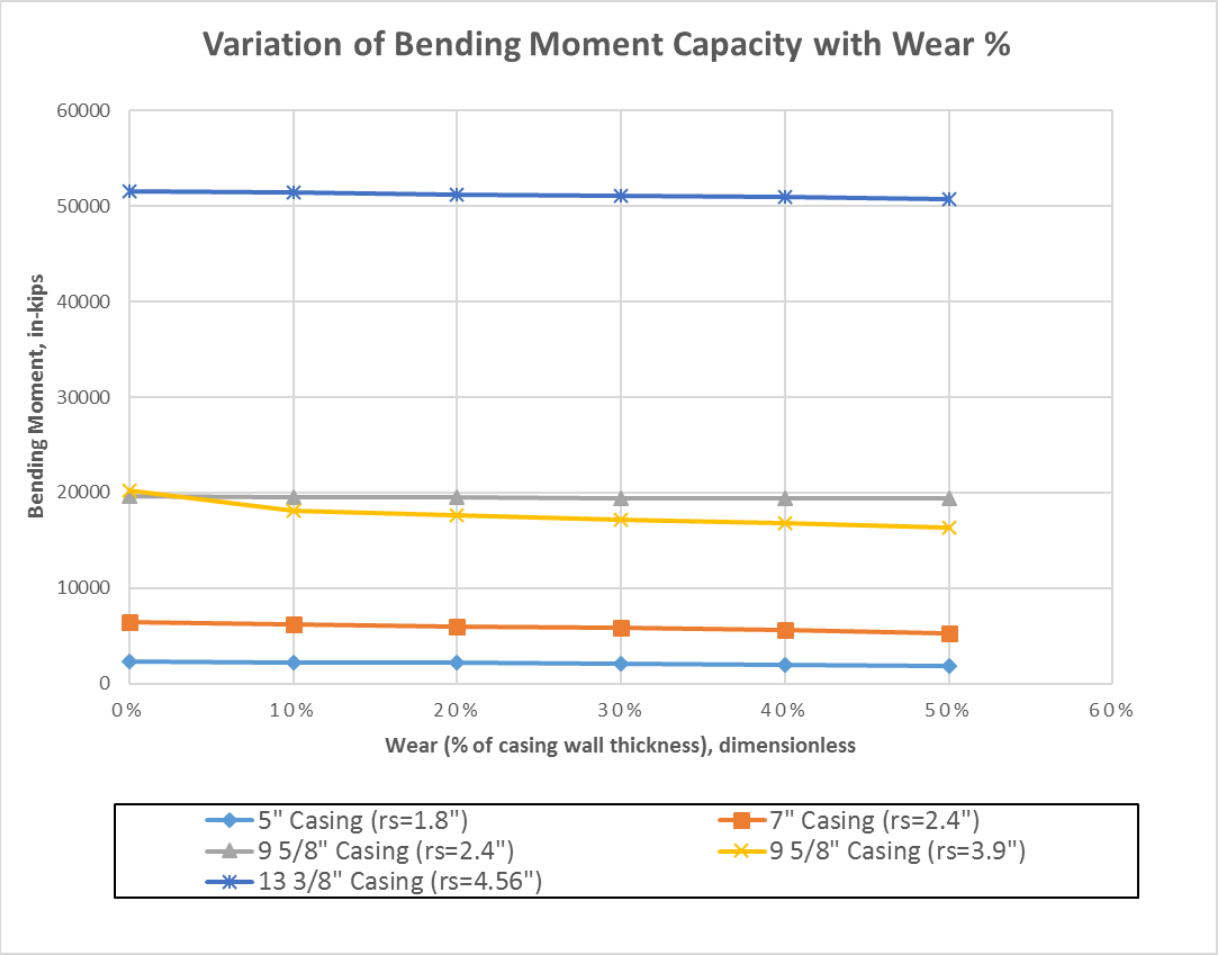

Figure 34: Plot showing bending moment capacity with wear for standard casing sizes

The bending moment capacities of all the commercial casing sizes with variation of casing wear percentages have been plotted as shown in Figure 34.

By observing Figure 34 and Table 22 to Table 26, it can be said that the variation of Bending moment capacity is not very high in higher OD casings. However, in lower OD casings such as 5" and 7", the variation is about 15 % - 20 % which is considerable to account for calculations. Overall, due to wear there is not much variation in bending moment.

5.3 Collapse

In this section, the elastic collapse pressure values obtained using new proposed collapse analytical model have been compared with Finite Element Analysis Collapse Eigen buckling simulation results using FEM model.

5.3.1 Model Validation - Wear influence on collapse pressure

Table 27 presents the comparison of the results with FEA model for 5" OD casing with wear circle radius of 1.80". To introduce the eccentricity in casing, minimum thickness (t_a) of 0.25" and maximum thickness (t_b) of 0.47" are used for calculations. The comparison has been done by varying the casing wear as a percentage of casing wall thickness from 0% to 50%. The first three columns of Table 27 contain characteristic values, such as outside diameter, nominal wall thickness and wear circle radius. The fourth column indicates the corresponding wear as a percentage of casing wall thickness varying from 10% to 50%. The fifth and sixth has h and mean radius at a section. Seventh column has elastic collapse pressure values computed using the new proposed model (Equation 79) for non-uniform wall thickness and wear. The respective values from FEA simulation are shown in seventh column for comparison. The eight column shows the variation of the elastic collapse pressure obtained using new proposed model and the FEA model.

Table 27: Comparison of elastic collapse capacity using analytical and numerical model - 5" OD casing

Casing Diameter	Thickness	Wear circle radius	Wear	h	Rm	P	P FEM	Variation
Inches	Inches	Inches	%	Inches	Inches	psi	psi	%
5	0.362	1.80	0%	0.34	2.33	21692.38	21088	3%
			10%	0.32	2.34	17652.85	18200	3%
			20%	0.30	2.35	14439.43	16019	10%
			30%	0.28	2.36	12214.26	13970	13%
			40%	0.26	2.37	9615.17	12233	21%
			50%	0.24	2.38	7269.70	9623	24%

The elastic collapse pressure values for new proposed model and FEA simulation for 5” casing with wear radius of 1.8” is presented in Table 27 are plotted in Figure 35.

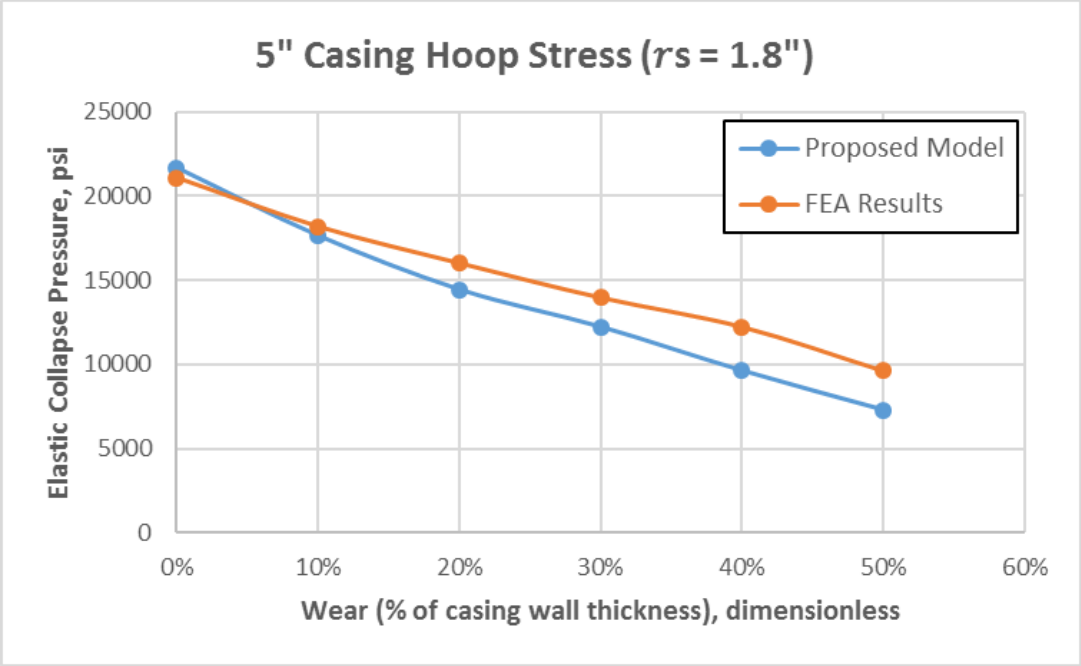

Figure 35: Plot showing comparison of elastic collapse capacity using analytical and numerical model - 5" OD casing

From Figure 35, results show the correlation between analytical and numerical methods, with the deviations between 3% and 24%. From this chart it is clear that both models show that with increase in wear percentage, the elastic collapse pressure decreases. The variation is increasing with the increase of wear percentage increases.

Table 28 presents the comparison of the results with FEA model for 7” OD casing with wear circle radius of 1.80”. To introduce the eccentricity in casing, minimum thickness (t_a) of 0.38” and maximum thickness (t_b) of 0.70” are used for calculations.

Table 28: Comparison of elastic collapse capacity using analytical and numerical model - 7" OD casing

Casing Diameter	Thickness	Wear circle radius	Wear	h	Rm	P	P FEM	Variation
Inches	Inches	Inches	%	Inches	Inches	psi	psi	%
7	0.540	2.40	0%	0.50	3.25	26486.59	26000	2%
			10%	0.47	3.26	21982.59	23588	7%
			20%	0.44	3.28	18054.17	20354	11%
			30%	0.42	3.29	14553.59	16335	11%
			40%	0.38	3.31	11394.83	13500	16%
			50%	0.36	3.32	9223.10	11295	18%

The elastic collapse pressure values for new proposed model and FEA simulation for 7" casing with wear radius of 2.4" as presented in Table 28 are plotted in Figure 36.

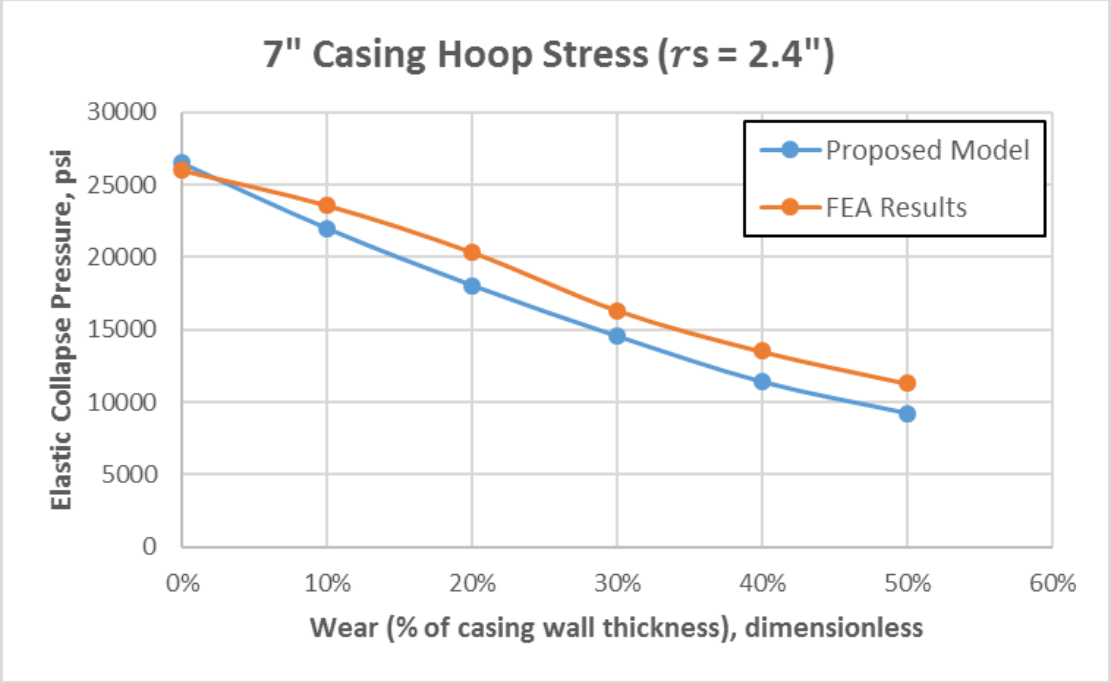

Figure 36: Plot showing comparison of elastic collapse capacity using analytical and numerical model - 7" OD casing

From Figure 36, results show the correlation between analytical and numerical methods, with the deviations between 2% and 18%. Similar to the previous casing analysis, the variation is increasing with the increase of wear percentage increases.

Table 29 presents the comparison of the results with FEA model for 9 5/8” OD casing with wear circle radius of 2.40”. To introduce the eccentricity in casing, minimum thickness (t_a) of 0.38” and maximum thickness (t_b) of 0.70” are used for calculations.

Table 29: Comparison of elastic collapse capacity using analytical and numerical model - 9 5/8" OD casing

Casing Diameter	Thickness	Wear circle radius	Wear	h	Rm	P	P FEM	Variation
Inches	Inches	Inches	%	Inches	Inches	psi	psi	%
9 5/8	0.540	2.40	0%	0.52	4.55	10826.18	10259	6%
			10%	0.49	4.57	9065.13	9504	5%
			20%	0.46	4.58	7285.58	8230	11%
			30%	0.44	4.59	6195.83	7122	13%
			40%	0.41	4.61	5010.00	6299	20%
			50%	0.38	4.62	4060.79	5145	21%

The elastic collapse pressure values for new proposed model and FEA simulation for 9 5/8” casing with wear radius of 2.4” is presented in Table 29 are plotted in Figure 37.

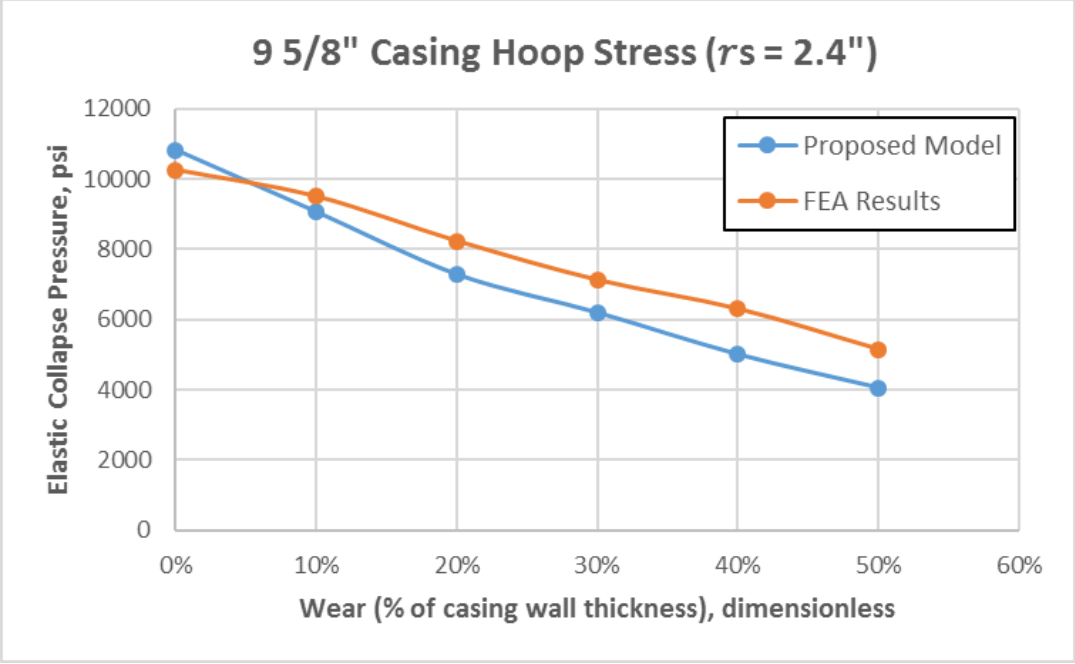

Figure 37: Plot showing comparison of elastic collapse capacity using analytical, numerical model - 9 5/8" OD casing

From Figure 37, results show the correlation between analytical and numerical methods, with the deviations between 6% and 21%. The variation is increasing with the increase of wear percentage increases.

Table 30 presents the comparison of the results with FEA model for 13 3/8" OD casing with wear circle radius of 4.56". To introduce the eccentricity in casing, minimum thickness (t_a) of 0.36" and maximum thickness (t_b) of 0.67" are used for calculations.

Table 30: Comparison of elastic collapse capacity using analytical and numerical model - 13 3/8" OD casing

Casing Diameter	Thickness	Wear circle radius	Wear	h	Rm	P	P FEM	Variation
Inches	Inches	Inches	%	Inches	Inches	psi	psi	%
13 3/8	0.514	4.56	0%	0.49	6.44	3186.45	3152	1%
			10%	0.46	6.46	2662.91	2900	8%
			20%	0.44	6.47	2224.99	2539	12%
			30%	0.41	6.48	1823.38	2180	16%
			40%	0.38	6.50	1422.25	1691	16%
			50%	0.35	6.51	1166.76	1412	17%

The elastic collapse pressure values for new proposed model and FEA simulation for 13 3/8" casing with wear radius of 4.56" is presented in Table 30 are plotted in Figure 38.

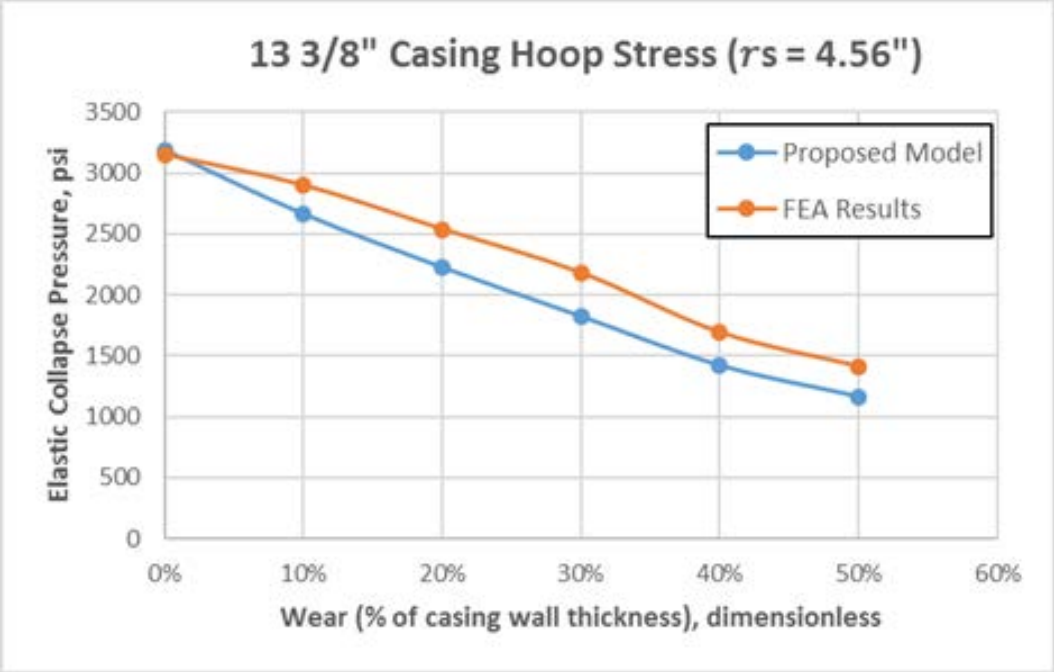

Figure 38: Plot showing comparison of elastic collapse capacity using analytical, numerical model - 13 3/8" OD casing

From Figure 38, results show the correlation between analytical and numerical methods, with the deviations between 1% and 17%. From this chart it is clear that both models show that with increase in wear percentage, the elastic collapse pressure decreases. The variation is increasing with the increase of wear percentage increases.

5.4 Guidelines to use the analytical models

To use the analytical models, firstly few things have to be identified. Based on the profile of the casing, the eccentricity or non-uniformity of the casing and maximum wear depth of the casing has to be identified. The other geometrically relevant parameters such as t_a , t_b, r_s, θ_o and α_o have to be evaluated. For burst, upon substituting the above mentioned values in equation (26), the maximum stress concentration factor for burst is obtained. Similarly, upon using these values in equations (59) and (79) the maximum bending capacity and collapse capacity of a non-uniform cylinder with wear can be calculated.

6 CONCLUSIONS

Analytical models have been developed for burst capacity, bending moment capacity and limit elastic buckling pressure for casing with wear in the bent cross section. The results from the analytical models have been validated with numerical simulations and subsequently compared against other existing models in the industry.

The following conclusions were reached from this study:

1. Proposed analytical and FEM simulated model comparison show a good correlation with a maximum deviation of 7%. It is easy to notice very good conformity between curves formed by the new proposed model and FEM results.
2. The new proposed model with constant thickness provides a higher inner pressure capacity than the API model which is based on the uniform wear model. The Nadai's model gives a higher pressure capacity compared to other models as it is based on ultimate tensile strength instead of yield strength. Very good conformity is formed between the new proposed model with constant thickness and crescent shape model.
3. Sensitivity analysis of casing wear percentage is performed in an attempt to understand the rate of strength degradation as a percentage of wear and wear circle radius for burst, collapse and bending. There is not much difference in results with wear circle.
4. Limit burst pressure calculations have been done by varying the thickness of the casing in the bent cross section.
5. It can be said that the variation of Bending moment capacity is not very high in higher OD casings. However, in lower OD casings such as 5" and 7", the variation is about 15 % - 20 % which is considerable to account for calculations. Overall, due to wear there is not much variation in bending moment.

6. Results show the correlation between collapse analytical and numerical model, with the deviations between 3% and 24%. The variation is increasing with the increase of wear percentage increases.
7. Re- assessment of limit burst, bending and collapse capacities for all the standard industry casing sizes using new proposed models.

7 LIMITATIONS AND FUTURE SCOPE

1. The developed analytical models can be used to create a model to calculate the failure point under combined loading of a non-uniform casing with wear.
2. A casing wear profile from the field data which exactly represents the drilling wear can be used to perform calculations.
3. The degradation of casing strength under combined axial and bending loading conditions should be calculated.
4. Casing collapse model should be modified to include cases where yielding starts before elastic buckling.
5. Hoop stress calculation of a thick walled pipe with including the effects of local bending.
6. A software program can be developed to create limit burst, collapse and bending capacities of a pipe with varying wall thickness profile, wear, sour conditions and combined loading as well.

REFERENCES

1. Li, C., & Samuel, R. (2016, March 1). “Casing Integrity: Modeling Strength Degradation. Society of Petroleum Engineers.” doi:10.2118/178791-MS
2. Sun, K., Samuel, R., & Guo, B. (2004, January 1). “Effect of Stress Concentration Factors due to Corrosion on Production Tubing Design.” Society of Petroleum Engineers. doi:10.2118/90094-MS
3. Kumar, A., & Samuel, R. (2015, March 17). “Casing Wear Factors: How do They Improve Well Integrity Analyses?” Society of Petroleum Engineers. doi:10.2118/173053-MS
4. Wu, J., & Zhang, M. (2005, January 1). “Casing Burst Strength After Casing Wear. Society of Petroleum Engineers.” doi:10.2118/94304-MS
5. Kuriyama, Y., Tsukano, Y., Mimaki, T., & Yonezawa, T. (1992, January 1). “Effect of Wear and Bending on Casing Collapse Strength.” Society of Petroleum Engineers. doi:10.2118/24597-MS
6. Kaldal, G.S., Jonsson, M.T., Palsson, H. and Karlsdottir, S.N., 2015. “Structural modeling of the casings in high temperature geothermal wells.” Geothermics, 55, pp.126-137.
7. Klever, F. J., & Tamano, T. (2006, September 1). “A New OCTG Strength Equation for Collapse Under Combined Loads.” Society of Petroleum Engineers. doi:10.2118/90904-PA
8. Hauch S, Bai Y. “Use of finite element methods for the determination of local buckling strength.” In: Proceedings of the 1998 International Conference on Offshore Mechanics and Arctic Engineering, Lisbon, Portugal, 5–9 July 1998.
9. Timoshenko SP, Gere JM. *Theory of elastic stability*. New York: McGraw-Hill, 1961.
10. API, 1994, “Bulletin on Formulas and Calculations for Casing, Tubing, Drill Pipe and Line Pipe Properties,” API Bulletin 5C3, 6th ed., API, Washington, DC.

11. Tamano, T., Mimaki, T., and Yanagimoto, S., 1983, “A New Empirical Formula for Collapse Resistance of Commercial Casing,” Proceedings of the Second International Offshore Mechanics and Arctic Engineering Symposium, ETCE, p. 489.
12. Clinedinst, W. O. (1939, January 1). “Rational Expression for the Critical Collapsing Pressure of Pipe under External Pressure.” American Petroleum Institute.
13. A. Nadai, *Plasticity*. McGraw-Hill, New York, NY (1931)
14. Bai Y, Igland R, Moan T. “Tube collapse under combined external pressure, tension and bending.” Mar. Struct. 1997;10(5):389–410.
15. Kuriyama, Y. (1994, January 1). “A New Formula for Elasto-Plastic Collapse Strength of Thick-Walled Casing.” Society of Petroleum Engineers. http:/doi:10.2118/28327-MS
16. Holmquist, J. L., & Nadai, A. (1939, January 1). “A Theoretical and Experimental Approach to the Problem of Collapse of Deep-Well Casing.” American Petroleum Institute.
17. Main, W. C. (1939, January 1). “Combining Bending and Hoop Stresses to Determine Collapsing Pressure of Oil-Country Tubular Goods.” American Petroleum Institute.

Appendix A

9 5/8 " Casing with 10% wear				9 5/8" Casing with 20% wear			
Node Number	Maximum Principal Stress (psi)	Nodes on thinnest cross-section	Corresponding Max. Principal Stress	Node Number	Maximum Principal Stress (psi)	Nodes on thinnest cross-section	Corresponding Max. Principal Stress
1	7463.1	2056	7086.6	1	4659.8	2063	2916.9
2	7395.8	44415	7470.5	2	4651	45832	3828.8
3	9282.4	38387	7854.4	3	6473	38783	4740.6
4	10256	95596	8221.3	4	7506.8	116913	5645.5
5	10923	26012	8588.2	5	8260.8	35602	6550.5
6	11489	89975	8951.2	6	8927	116671	7450.2
7	11984	23326	9314.3	7	9539.2	35483	8349.9
8	12443	85282	9696.9	8	10115	113794	9248
9	12875	21076	10079	9	10673	34086	10146
10	13288	82364	10450	10	11223	110901	11050
11	13689	19667	10820	11	11774	32693	11955
12	14082	82365	11194	12	12325	108057	12856
13	14465	22356	11567	13	12871	31317	13756
14	14839	87966	11959	14	13418	102469	14651
15	15204	25055	12350	15	13969	28591	15546
16	15563	93568	12758	16	14522	99614	16448
17	15914	35282	13166	17	15084	27199	17350
18	16258	114763	13582	18	15651	99509	18263
19	16595	35306	13998	19	16214	27150	19176
20	16928	114812	14436	20	16780	99510	20106
21	17253	35313	14874	21	17346	41444	21036
22	17569	114827	15331	22	17914	39867	8019
23	17872	35342	15787	23	18485	24445	22909
24	18161	114885	16261	24	19060	91109	23838
25	18438	35359	16735	25	19632	23118	24768
26	18703	114918	17224	26	20195	90399	25713
27	18955	35361	17713	27	20754	22790	26658
28	19195	114922	18219	28	21308	90400	27609
29	19420	35377	18725	29	21856	38893	28560
30	19631	114957	19256	30	22398	41817	29618
31	19828	36532	19786	31	22934	55	30676
32	20010	40388	20347	32	23468		
33	20176	42	20908	33	23992	**Max. P Stress**	**16110.88**
34	20327			34	24500		
35	20462	**Max. P Stress**	**13476.01**	35	24991		
36	20580			36	25468		
37	20680			37	25931		
38	20762			38	26378		
39	20827			39	26807		
40	20872			40	27216		
∫	∫			∫	∫		
119556	5811.2			119556	13215		
119557	8428.2			119557	13348		
119558	5827.5			119558	13235		
119559	8259.3			119559	13370		